ISPRS Journal of Photogrammetry and Remote Sensing 125 (2017) 156–173

Contents lists available at ScienceDirect

ISPRS Journal of Photogrammetry and Remote Sensing

journal homepage: www.elsevier.com/locate/isprsjprs

Accuracy assessment of seven global land cover datasets over China

Yongke Yang, Pengfeng Xiao *, Xuezhi Feng, Haixing Li

Department of Geographic Information Science, Nanjing University, Nanjing, Jiangsu 210023, China
Collaborative Innovation Center of South China Sea Studies, Nanjing, Jiangsu 210023, China
Jiangsu Center for Collaborative Innovation in Geographical Information Resource Development and Application, Nanjing, Jiangsu 210023, China

ARTICLE INFO

Article history:
Received 28 June 2016
Received in revised form 22 December 2016
Accepted 24 January 2017

Keywords:
Global land cover dataset
Spatial agreement
Accuracy validation
Spatial variation in accuracy

ABSTRACT

Land cover (LC) is the vital foundation to Earth science. Up to now, several global LC datasets have arisen with efforts of many scientific communities. To provide guidelines for data usage over China, nine LC maps from seven global LC datasets (IGBP DISCover, UMD, GLC, MCD12Q1, GLCNMO, CCI-LC, and GlobeLand30) were evaluated in this study. First, we compared their similarities and discrepancies in both area and spatial patterns, and analysed their inherent relations to data sources and classification schemes and methods. Next, five sets of validation sample units (VSUs) were collected to calculate their accuracy quantitatively. Further, we built a spatial analysis model and depicted their spatial variation in accuracy based on the five sets of VSUs. The results show that, there are evident discrepancies among these LC maps in both area and spatial patterns. For LC maps produced by different institutes, GLC 2000 and CCI-LC 2000 have the highest overall spatial agreement (53.8%). For LC maps produced by same institutes, overall spatial agreement of CCI-LC 2000 and 2010, and MCD12Q1 2001 and 2010 reach up to 99.8% and 73.2%, respectively; while more efforts are still needed if we hope to use these LC maps as time series data for model inputting, since both CCI-LC and MCD12Q1 fail to represent the rapid changing trend of several key LC classes in the early 21st century, in particular urban and built-up, snow and ice, water bodies, and permanent wetlands. With the highest spatial resolution, the overall accuracy of GlobeLand30 2010 is 82.39%. For the other six LC datasets with coarse resolution, CCI-LC 2010/2000 has the highest overall accuracy, and following are MCD12Q1 2010/2001, GLC 2000, GLCNMO 2008, IGBP DISCover, and UMD in turn. Beside that all maps exhibit high accuracy in homogeneous regions; local accuracies in other regions are quite different, particularly in Farming-Pastoral Zone of North China, mountains in Northeast China, and Southeast Hills. Special attention should be paid for data users who are interested in these regions.

1. Introduction

Land cover (LC) is one of the indispensable variables for the study of Earth system process. It provides thematic information of the Earth's surface that captures biotic and abiotic properties closely tied to the ecological condition of land areas (Friedl et al., 2010). LC mapping has been considered as the most important agent research on environmental change and sustainability (Foley et al., 2005; Running, 2008; Gong et al., 2013; Zhang et al., 2014).

To date, nine global LC datasets have arisen from different initiatives using satellite data, i.e. (1) International Geosphere-Biosphere Program Data and Information System's LC dataset (IGBP DISCover), 1992–1993, 1 km resolution (Loveland and Belward, 1997; Loveland et al., 2000), (2) University of Maryland LC dataset (UMD), 1992–1993, 1 km resolution (Hansen et al., 2000), (3) Global LC 2000 dataset (GLC) from the European Commission's Joint Research Center (JRC), 1 km resolution (Bartholomé and Belward 2005), (4) Moderate Resolution Imaging Spectroradiometer (MODIS) LC dataset (MOD12Q1 and MCD12Q1) available at annual scale from 2001, 500/1000 m resolution (Friedl et al., 2002; Friedl et al., 2010), (5) Global LC Map (GlobCover) from European Space Agency (ESA), 2005–2006/2009, 300 m resolution (Arino et al., 2008; Bontemps et al., 2010), (6) Climate Change Initiative LC dataset (CCI-LC) from ESA, 2000/2005/2010, 300 m resolution (Defourny et al., 2016), (7) Global Map–Global LC (GLCNMO) dataset from the International Steering Committee for Global Mapping, 2003/2008, 500 m resolution (Tateishi et al., 2014), (8) Finer Resolution Observation and Monitoring Global LC dataset (FROM-GLC) from China based on Landsat images from 1984 to 2011, 30 m

* Corresponding author at: Department of Geographic Information Science, Nanjing University, Nanjing, Jiangsu 210023, China.
E-mail address: xiaopf@nju.edu.cn (P. Xiao).

http://dx.doi.org/10.1016/j.isprsjprs.2017.01.016
0924-2716/

resolution (Gong et al., 2013; Yu et al., 2013), and (9) 30 m resolution Global LC dataset (Globeland30) from National Geomatics Center of China, 2000/2010 (Chen et al., 2015).

Although these LC datasets provide a typically reflection of the Earth's surface, there must be some differences among these LC datasets derived from different satellite data, classification scheme and approach. Thus, accuracy assessment is needed for better using of these LC datasets. The literature of existing accuracy assessment works for these LC datasets are listed in Table 1. Two commonly used methods for accuracy assessment of LC datasets are (1) crossing with validations sample pixels within a confusion matrix, and (2) measuring agreement and disagreement with existing LC maps or statistical LC information. E.g., the overall accuracies were derived from confusion matrices for the following maps: 66.9% for IGBP DISCover (Scepan et al., 1999), 68.6% for GLC 2000 (Mayaux et al., 2006), 78.3% for MCD12Q1 2010 (Friedl et al., 2002), 77.9% for GLCNMO 2008 (Tateishi et al., 2014), 73.2% for CCI-LC (Defourny et al., 2016), 64.9% for FROM-GLC (Gong et al., 2013), and 80.3% for GlobeLand30 (Chen et al., 2015). Besides, some studies show that there are large areas of disagreement among these datasets, e.g. in the west of China (Giri et al., 2005; Herold et al., 2008; McCallum et al., 2006).

Many efforts have been paid by Chinese scientists to evaluate the accuracies of the global LC datasets over China. E.g., Wu et al. (2008) and Ran et al. (2010) validated IGBP DISCover, UMD, MOD12Q1 2001, and GLC 2000 using the same validation database, i.e. China's LC map of 2000 produced by Liu et al. (2003), respectively. The results of the former indicate that MOD12Q1 2001 has the best fit in depicting China's croplands. The results of the later indicate that GLC 2000 has the highest overall accuracy (59.3%). Niu et al. (2012) assessed the accuracy of wetlands in GlobCover 2009 using the wetland map of China in 2008, and found that the overall accuracy of wetlands in GlobCover 2009 is only 32.0%, and the wetland area of GlobCover 2009 is far smaller than that in reference data. Note that some global LC datasets use a regional stratification classification approach (e.g. IGBP DISCover, GLC, GLCNMO, and CCI-LC), so that their accuracy over China may not be identical elsewhere. Moreover, in the case that FROM-GLC and GlobeLand30 were produced by Chinese institutes, their accuracy over China can be expected to be higher.

Table 1
Literature of existing accuracy assessment works for global LC datasets.

Validation method	LC dataset	Literature
Crossing with validation sample pixels (measuring overall accuracy, producer's and user's accuracy, and Kappa coefficient)	IGBP DISCover	Scepan et al. (1999)
	GLC	Mayaux et al. (2006)
	GlobCover	Bicheron et al. (2008)
	CCI-LC	Defourny et al. (2016)
	GLCNMO	Tateishi et al. (2014)
	IGBP DISCover, UMD, GLC, MODIS	Latifovic and Olthof (2004), Herold et al. (2008)
	IGBP DISCover, UMD, MODIS	Gong (2009)
	FROM-GLC	Gong et al. (2013)
	GlobeLand30	Chen et al. (2015)
	MODIS	Friedl et al. (2002)
Measuring agreement/ disagreement with existing LC maps or statistical data	IGBP DISCover and UMD	Hansen and Reed (2000)
	GLC and MODIS	Fritz and See (2008), Fritz et al. (2010), Gao and Jia (2012)
	IGBP DISCover, UMD, GLC, MODIS	McCallum et al. (2006), Jung et al. (2006), Wu et al. (2008), Ran et al.(2010)
	MODIS	Sedano et al. (2005)
	GLC, MODIS, GlobCover	Tchuenté et al. (2011)
	IGBP DISCover, UMD, GLC, MODIS, GlobCover	Pérez-Hoyos et al. (2012a); Kuenzer et al. (2014)
	GlobCover	Niu et al. (2012), An et al. (2012)

Unfortunately, these existing works did not refer to the accuracy of evergreen needleleaf forests, evergreen broadleaf forests, deciduous needleleaf forests, deciduous broadleaf forests, mixed forests, cropland/natural vegetation mosaic, and snow and ice over. Since there is no available LC map of China containing these LC classes and it is expensive and time-consuming to collect new validation database. However, it is meaningful to obtain a more detailed description about the accuracies of these global LC datasets.

While valuable for guiding data usage, existing accuracy information, e.g. the accuracy indexes derived from confusion matrix, provides only a global estimation for the entire map, and does not represent the spatial variation in classification errors (Foody, 2002; Foody, 2005; Strahler et al., 2006; Comber et al., 2012). Instead of being random or stationary in space, however, the classification errors may vary within map area (Campbell, 1981; Steele et al., 1998; Foody, 2005). Many users, especially those only interested in parts of the mapped area or those using maps within spatially distributed models, may benefit from a spatial analysis of the classification accuracy (Kyriakidis et al., 1999; Strahler et al., 2006). Thus, describing the spatial variation of classification accuracy is one of our motivations for this study.

The existing methods used to describe the spatial variation in classification accuracy can be divided into two types: (1) confidence-based method (generate a strength map of the class membership) (Maselli et al., 1994; Colditz et al., 2012; Pérez-Hoyos et al., 2012b), and (2) geo-statistically based method (Congalton, 1988; Meer, 1996; Atkinson and Lewis, 2000; Kyriakidis and Dungan, 2001; Foody, 2005; Comber et al., 2012). The former method is based on the development of a confidence map to describe the spatial variation in classification errors. However, as an ancillary dataset provided by data producers, confidence map can only be obtained along with the development of the LC map. The later has been proved to be an available and meaningful method to depict the spatial variation in classification errors. E.g., Foody (2005) attempted to compute local accuracy of a LC map by geographically constraining the validation samples used for each target location. Comber et al. (2012) used a local binary logistical regression method to reveal the local accuracy. For each target location, a kernel function was applied to define validation sample and weighting used for local accuracy assessment; thus the parameter is a dynamic variables related to the geographic space rather than constants.

The goal of this study is to evaluate the similarities and differences of these global LC datasets, and their classification accuracy over China, by conducting a comparative assessment through three aspects: (1) comparing the areal and spatial agreement among different LC maps, and analysing their inherent relation with data sources and classification schemes and methods, (2) calculating the overall accuracy, user's and producer's accuracy, and Kappa coefficient for each LC maps based on the validation samples, which are collected by visual interpretation of high resolution images, and (3) depicting the spatial variations in classification accuracy for each LC maps via a geographically weighted statistical model.

2. Data and methodology

2.1. Global land cover datasets

This study refers to nine LC maps (IGBP DISCover, UMD, GLC 2000, MCD12Q1 2001, MCD12Q1 2010, GLCNMO 2008, CCI-LC

2000, CCI-LC 2010, and GlobeLand30 2010) from seven global LC datasets, in which two datasets (MCD12Q1 and CCI-LC) have respectively two maps of different year. Besides, two old versions of updated datasets (GlobCover and FROM-GLC) are not considered in this study. All maps were freely downloaded, and were re-projected into Lambert conformal conic projection and clipped by China's national boundaries uniformly for subsequent processing.

FROM-GLC and GlobeLand30 are two products of the Global LC mapping project aimed at developing a 30 m global LC dataset (Chen et al., 2015). FROM-GLC is the first product produced by Support Vector Machine classifier using Landsat images, with an overall accuracy of 64.9%, and it is also the first global LC dataset with 30 m resolution (Gong et al., 2013). Unlike the automated classifier used in FROM-GLC, GlobeLand30 was produced by Pixel-Object-Knowledge-based (POK-based) method, for the purpose of generating a 30-m global LC dataset with a higher accuracy than FROM-GLC (Chen et al., 2015). POK-based approach means an integration of a pixel- and object-based classification method, and knowledge-based interaction verification of the classification result. The validation results show that the overall accuracy of GlobeLand30 2010 reaches to 80.3% (Chen et al., 2015). Thus, only GlobeLand30 2010 was considered in this study. Another reason that FROM-GLC was not considered is that it was produced based on thousands of Landsat images during 1981–2011. Thus, it is inappropriate to compare it with other global LC maps at specific year.

GlobCover and CCI-LC are two LC datasets produced by two different projects leaded by ESA using MEdium Resolution Imaging Spectrometer (MERIS) images. Note that CCI-LC was built upon the GlobCover project experiences. Such as the pre-processing and the classification module used in CCI-LC are all coming from the GlobCover project, while these modules will be improved according to the requirements of the CCI-LC project; and GlobCover is one of the auxiliary datasets used in CCI-LC to define training areas for supervised classification and to label clusters generated by unsupervised classification. To meet the requirements of the climate community, CCI-LC have three advantages compared to GlobCover: (1) CCI-LC used a more detailed classification scheme, e.g., lichens and mosses were added into the classification scheme of CCI-LC, since it is extremely sensitive to climate; (2) to improve the accuracy of water bodies in CCI-LC, the Advanced Synthetic Aperture Radar (ASAR) at a 150 m resolution was used to generate more accurate water bodies; (3) three LC maps at different year from CCL-LC shows high stability, which is extremely important when time series of LC datasets are needed for model input (Defourny et al., 2016). For the reasons above, GlobCover was not considered in this study.

Besides, MODIS LC dataset contains two versions, i.e. MOD12Q1 (1 km) and MCD12Q1 (500 m), thus we just choose the latest and higher-resolution version MCD12Q1. In addition, although both CCI-LC and MCD12Q1 have datasets for more than one phase, e.g. MCD12Q1 is available at annual scale from 2001, and CCI-LC is available for 2000, 2005, and 2010, only maps at same or close phase were considered in this study, i.e. MCD12Q1 2001 and 2010, CCI-LC 2000 and 2010.

The LC maps involved in this study can be divided into three epochs: 1992–1993 (IGBP DISCover, UMD), 2000–2001 (GLC 2000, MCD12Q1 2001, CCI-LC 2000), and 2008–2010 (GLCNMO 2008, MCD12Q1 2010, CCI-LC 2010, GlobeLand30 2010). These LC maps provide a synoptic view of the global LC mapping efforts of the past decades. Table 2 shows the satellite data, classification scheme and method applied in different LC maps.

A uniform classification scheme is the basis of comparison analysis of different LC maps. Classification schemes used in IGBP DISCover, UMD, MCD12Q1 are all based on IGBP scheme; while classification scheme used in CCI-LC and GLCNMO2008 is the LC

Table 2
Characteristics of the nine global LC maps.

LC Map	IGBP DISCover	UMD	GLC 2000	MCD12Q1 2001/2010	GLCNMO 2008	CCI-LC 2000/2010	GlobeLand30 2010
Satellite sensor	NOAA AVHRR	NOAA AVHRR	SPOT VGT	Terra and Aqua MODIS	Terra and Aqua MODIS	ENVISAT MERIS SPOT VGT	Landsat TM/ETM+, HJ-1
Input data	12 monthly NDVI composites	41 metrics derived from NDVI and 5 spectral bands	Daily data consist of 4 spectral bands and NDVI	16-day nadir BRDF adjusted reflectance, 7 spectral bands, EVI	16-day nadir BRDF adjusted reflectance, 7 spectral bands, DMSP-OLS, Landsat ETM +	MERIS 7-day composite surface reflectance, SPOT VGT time series data	Optical bands in TM/ETM + and HJ-1, some auxiliary, e.g. MODIS NDVI time series data
Spatial resolution	1 km	1 km	1 km	500 m	500 m	300 m	30 m
Date of satellite data	1992.4–1993.3	1992.4–1993.3	1999.11–2000.12	2001.1–2001.12/ 2010.1–2010.12	2008.1–2008.12	Centred on year 2000/2010	Mainly in 2010
Classification scheme	IGBP (17 classes)	IGBP (14 classes)	LCCS (22 classes)	IGBP (17 classes)	LCCS (20 classes)	LCCS (22 classes)	10 classes
Classification strategy and method	The Earth was divided into 5 continents, and each continent was classified separately using k-means method	The Earth was viewed as an entirety and classified via decision tree method	The Earth was divided into 19 regions, each region was classified alone. China was dived into 9 regions, each region was classified by ISODATA method	The Earth was viewed as an entirety and was classified using the decision tree method.	The Earth was divided to 6 regions, and was classified separately by decision tree method	The earth was divided into 22 climatic regions, and each region was classified separately by the combination of use of the supervised and unsupervised method.	The Earth was divided into equal map sheet and classified separately by the combination of pixel- and object-based method.

Classification System (LCCS) produced by Food and Agriculture Organization of United Nations; GlobeLand30 adopted a classification scheme determined by Chen et al. (2015). The schemes used in these datasets differ greatly in term of categories, thresholds of vegetation canopies, and height limitations (Table 3). In order to facilitate the comparative analysis, it is common to convert LCCS scheme into IGBP scheme (Giri et al., 2005; McCallum et al., 2006; Kuenzer et al., 2014). In this study, we also selected IGBP as basis scheme, and converted LCCS scheme into IGBP scheme. Lichens and mosses in CCI-LC and tundra in GlobeLand30 were not compared, because there are no corresponding classes in IGBP scheme.

2.2. Comparison analysis

Comparison analysis contains two aspects: area comparison and spatial comparison. Area comparison emphasizes the area differences of individual classes in the different LC datasets. Spatial comparison also includes two aspects, i.e. visual comparison and per-pixel comparison. Visual comparison highlights the similarities and differences of the spatial patterns for each class. By conducting per-pixel comparison, pixels with the same LC class in different datasets retain their values, whereas pixels with a different LC class will be labeled as a disagreement. Furthermore, two agreement measures, overall spatial agreement (A_O) and

Table 3
Classification schemes employed in the seven global LC datasets. The LCCS and other schemes are converted to match to the IGBP scheme.

Class ID	IGBP DISCover/MCD12Q1	UMD	GLC	GLCNMO	CCI-LC	GlobeLand30
1	Evergreen needleleaf forests (>60%)	Evergreen needleleaf forests (>60%)	Tree cover, needle-leaved, evergreen (>15%)	Needleleaf evergreen forest (>40%)	Tree cover, needleleaved, evergreen, closed to open (>15%)	Forest
2	Evergreen broadleaf forests (>60%)	Evergreen broadleaf forests (>60%)	Tree cover, broad-leaved, evergreen (>15%)	Broadleaf evergreen forest (>40%)	Tree cover, broadleaved, evergreen, closed to open (>15%)	
3	Deciduous needleleaf forests (>60%)	Deciduous needleleaf forests (>60%)	Tree cover, needled-leaved, deciduous (>15%)	Needleleaf deciduous forest (>40%)	Tree cover, needleleaved, deciduous, closed to open (15%)	
4	Deciduous broadleaf forests (>60%)	Deciduous broadleaf forests (>60%)	Tree cover, broadleaved, deciduous (>40%) Tree cover broadleaved, deciduous (15–40%)	Broadleaf deciduous forest (>40%)	Tree cover, broadleaved, deciduous, closed to open (>15%)	
5	Mixed forests (each forest type cover <60%)	Mixed forests (each forest type cover <60%),	Tree cover, mixed leaf type (>15%)	Mixed forest (>40%) Open tree (10–40%)	Tree cover, mixed leaf type (broadleaved or needleleaved)	
6	Shrublands (closed and open,>10%)	Shrublands (closed and open,>10%)	Shrub, closed to open, evergreen (>15%) Shrub, closed to open, deciduous (>15%)	Shrub (>40%)	Shrubland (evergreen shrubland, deciduous shrubland)	Shrubland
7	Woody savannas (lands with herbaceous and other understory system and with forest canopy cover between 30–60%)	Woodland (lands with herbaceous or understory woody, and with tree canopy cover between 40–60%)	Mosaic tree cover/other natural vegetation	–	Mosaic tree and shrub (>50%)/ herbaceous cover (<50%)	–
8	Savannas (lands with herbaceous and other understory system and with forest canopy cover between 10–30%)	Wooded grassland (lands with herbaceous and tree cover between 10–40%)	–	Herbaceous (>40%) with sparse tree/ shrub,	Mosaic herbaceous cover (>50%)/tree and shrub (<50%)	–
9	Grasslands (>10%)	Grasslands (>10%)	Herbaceous cover, closed to open (>15%)	Herbaceous (>40%),	Grassland	Grassland
10	Permanent wetlands	–	Tree cover, regularly flooded, fresh water, Tree cover, saline water regularly flooded; Regularly flooded shrub or herbaceous cover;	Wetland; Mangrove;	Tree cover, flooded, fresh or brackish water; Tree cover, flooded, saline water; Shrub or herbaceous cover flooded, fresh/ saline/rakish water;	Wetland
11	Croplands	Croplands	Cultivated and managed areas	Cropland; Paddy field;	Cropland, rained Cropland, irrigated or post flooding	Cultivated land
12	Urban and built-up	Urban and built	Artificial surfaces and associated areas	Urban	Urban areas	Artificial surfaces
13	Cropland/natural vegetation mosaic	–	Mosaic cropland/tree/other natural vegetation; Mosaic cropland/shrub or grass cover; Mosaic tree cover/other vegetation;	Cropland /other vegetation mosaic;	Mosaic cropland (> 50%)/natural vegetation (<50%); Mosaic natural vegetation (> 50%)/cropland (<50%);	–
14	Snow and ice	–	Snow and ice	Snow/ice	Snow and ice	Snow and ice
15	Barren (<10%)	Barren (<10%)	Sparse herbaceous or sparse shrubland Bare areas (<15%)	Bare, consolidated; Bare, unconsolidated; Sparse vegetation;	Sparse vegetation (tree, tree, herbaceous cover) (<15%); Bare areas (consolidated area, unconsolidated area);	Barre land
16	Water bodies	Water	Water bodies	Water bodies	Water bodies	Water bodies

The content in '( )' is the threshold of vegetation canopy for each class, '–' indicates that the class is absent in the LC dataset.

individual-class spatial agreement (A_i), will be calculated using the following equations:

$$A_O = \frac{\sum_{1}^{N} XY_{ii}}{M} \times 100\% \quad (1)$$

$$A_i = \frac{XY_{ii}}{(X_i + Y_i)/2} \times 100\% \quad (2)$$

where X_i is the number of pixels of class i in dataset X, Y_i is the number of pixels of class i in dataset Y, XY_{ii} is the number of pixels of class i in both X and Y, N is the number of classes used to calculate overall spatial agreement, and M is the total number of pixels in the study area.

2.3. Collection of validation sample units

Five sets of validation sample units (VSUs) were collected via visual interpretation of high resolution images on Google Earth (GE). High resolution images on GE have become an vital data for accuracy assessment (Clark et al., 2010; Friedl et al., 2010; Bicheron et al., 2011; Defourny et al., 2016). Its obvious advantage in collecting VSUs are: (1) it provides free access to high resolution images; (2) it can provide a synoptic views of the sampling plot at different angles and scales; (3) spatial error of the high resolution images on GE is low, only about 15 ± 5 m (Clark et al., 2010); (4) the timeline of GE can be used to check images at different phase, and help us to identify LC class with seasonal characteristic, i.e. evergreen needleleaf forest, deciduous needleleaf forest, evergreen broadleaf forest, deciduous broadleaf forest, and (5) panoramic photos on GE can provide an ancillary reference for interpretation of high resolution images.

The five sets of VSUs and the matching LC maps to be evaluated are shown in Table 4. Ideally, the phase of the VSUs should match that of the LC maps to be evaluated. However, it is impossible to collect VSUs of 1992–1993 via GE directly, since the high resolution images on GE mainly appeared after 2000. A compromise solution is to evaluate the accuracy of IGBP DISCover and UMD using VSUs of 2000–2001. One question, that is, how did the LC in China change from 1992 to 2001, must be answered to confirm whether the VSUs of 2000–2001 could represent the Earth's surface and assess the accuracy of LC maps in 1992–1993. Some existing studies show that the total area of LC change in China in the 1990s was only 0.5% of the land area, in other words, LC classes of the most parts of China are stable in the 1990s; and the LC change mainly happens in (1) traditional agricultural regions, e.g. the Huang-Huai-Hai Plain and Yangtze Delta, where cropland decreased obvious due to urbanization, (2) the agriculture and nomadic areas, where grassland were cultivated into croplands (Liu et al., 2003; Li et al., 2005; Liu et al., 2014), and (3) the Northeast China, logging activities in Da Hinggan Ling (main forest class is larch forest) and Xiao Hinggan Ling (main forest class is mixed needleleaf-broadleaf forests) result in an ongoing loss of forest, with a percent <5% of the total forest area in Northeast China during the late 1990s (Achard et al., 2006). Thus one hypothesis is that VSUs of 2000–2001 could be used to validate IGBP DISCover and UMD if they were collected from regions without change.

Table 4
Five sets of VSUs and the corresponding LC maps to be evaluated.

No.	Set of VSUs	LC map
1	VSUs of 2000–2001 (2 km × 2 km)	IGBP DISCover 1992–1993 UMD 1992–1993 GLC 2000
2	VSUs of 2000–2001 (1 km × 1 km)	MCD12Q1 2001
3	VSUs of 2000–2001 (600 m × 600 m)	CCI-LC 2000
4	VSUs of 2008–2010 (1 km × 1 km)	GLCNMO 2008 MCD12Q1 2010
5	VSUs of 2008–2010 (600 m × 600 m)	CCI-LC 2010 GlobeLand30 2010

The content in "( )" is the size of the VSU.

Another issue need to be considered is the size of the VSU should fit the pixel size of the LC map to be evaluated. The size of VSU was defined as 2 × 2 pixels of the LC map to be evaluated. On one side, the validation result will be easily affected by the inherent location errors of satellite imaging, if the size of VSU is just equal to a single pixel (Mayaux et al., 2006). On the other side, more uncertainty coming from the landscape heterogeneity will be introduced into VSU, if the size of VSU is too large.

Fig. 1 is the detailed workflow of the collection for five sets of VSUs. With considerations of all issues mentioned above, VSUs of 2000–2001 (2 km × 2 km) were collected by the following four steps:

Step 1: Building a LC change map to find regions without LC change during the 1990s. Two LC maps of China (1990 and 2000) provided by Liu et al. (2003) were used to obtain the change map. After then, the change map was overlaid on GE as a mask to find regions without LC change. Only high resolution images located in these regions were considered for collecting VSUs. In general, it will introduce a bias to the assessing result if all VSUs were selected from regions without LC change. However, this effect is very slight, e.g. the region that LC change in China during the 1990s accounts for only 0.5% of the land area (Liu et al., 2003). The two LC maps of China (1990 and 2000) were produced based on visual interpretation and digitization process using mainly TM images. The overall accuracies, valuated by a nationwide field surveys in all provinces except Tibet and Taiwan, is 97.5% and 92.9% for map of 2000 and 1990, respectively. The accuracy of changed polygons in the 1990s is greater than 95%. It has been the main source of authoritative data for LC change studies of China (Zhang et al., 2014).

Step 2: Creating a 1-km grid to match the 1-km LC map, and overlaying the grid with the high resolution (HR) images on GE. Then it will be used to ensure that the size of VSU is exactly 2 km × 2 km.

Step 3: Collecting VSUs visually by nine land cover experts participating in the project based on the high resolution images on GE. The vegetation map of China at a scale of 1:1,000,000 produced by Hou (2001) and the 1-km LC map in 2000 produced by Liu et al. (2003) were used to help the nine experts obtain an overview of the spatial pattern of each class, before visually selecting the VSUs. Then a VSU will be collected when a high resolution image is found in the target regions, and class of all four pixels of the VUS with size of 2 km × 2 km are the same. The land cover types of the four pixels of the VUS was judged through visual interpretation by the land cover experts, and a report was created by each expert to record four kinds of information related to each VSU, i.e. LC class, high resolution images, panoramic photos, and spatial location. These reports will be used to verify the reliability of VSUs. Noted that there are two unavoidable limitations of the VSUs, (1) although we tried to make the VSUs normally distributed in the entire study area, it will introduce unknown bias since the VSUs were selected from an empirical instead of a statistical valid manner; and (2) for classes with small patch size or with long but narrow shape, e.g. water bodies, most of the rivers in China are excluded from the VSU, since the rivers are often too narrow to select a VSU with size of 2 km × 2 km; i.e. the VSUs of water bodies are often selected from lakes more than 4 km^2 size, so that the accuracy of water bodies obtained from this study may be higher than the real accuracy, since large water bodies are easier to map.

Step 4: Verifying the reliability of the VSUs. Interpretation error caused by each expert is the major factor that affects the quality of

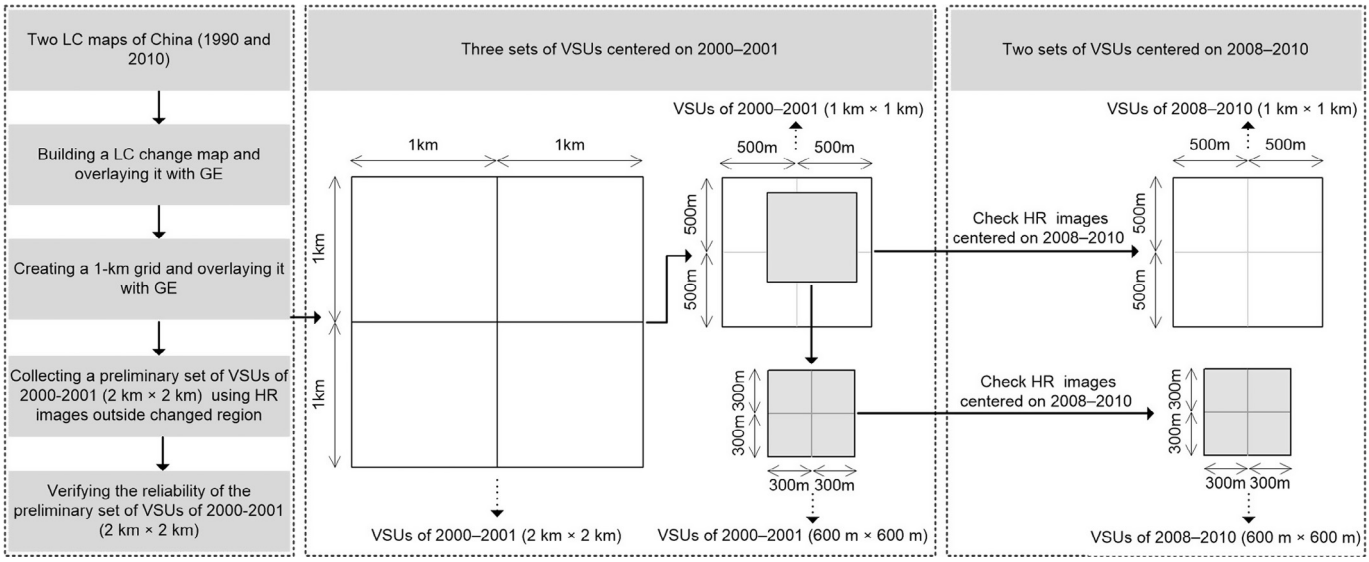

Fig. 1. Workflow of the collection for five sets of VSUs. The VSU with size of 1 km × 1 km is one of the four pixels of the VSU with size of 2 km × 2 km. The VSU with size of 600 m × 600 m is not centered in the VSU size of 1 km × 1 km. It depends on the actually location.

VSUs. To minimize this error, one commonly used method is to check these VSUs again by different experts, and to adopt the opinion with high agreement. Thus, the nine experts were gathered together to take a project meeting, so that they can discuss and exchange their opinions face to face. The reports produced in step 3 were used to exhibit each VSU one by one. All experts expressed their opinions for each VSU according to the four kinds of information recorded in each report. Only those VSUs that more than 6/9 experts show the same opinion to the LC class were considered for inclusion of the set of VSUs 2000–2001 (2 km × 2 km) finally.

Next, the VSUs of 2000–2001 (2 km × 2 km) were regarded as a baseline to collect VSUs of 2000–2001 (1 km × 1 km). We created a 500-m grid to match MCD12Q1 2001, and overlaid the grid with the VSUs of 2000–2001 (2 km × 2 km). Then, a new set of VSUs with size of 1 km × 1 km located in the 2 km × 2 km base was collected. Before collecting the new set of VSUs, we checked the high resolution images it covers again, which is important for the mixed forest and cropland/natural vegetation mosaic. E.g., a 1-km pixel, with half of 500-m pixels are needleleaf forest, and half of other 500-m pixels are broadleaved forest, will be assigned as mixed forest; while error will be introduced if all four 500-m pixels within it were labeled as mixed forest. If so, a new VSU will be collected near the original one.

The VSUs of 2008–2010 (1 km × 1 km) were derived from the VSUs of 2000–2001 (1 km × 1 km). Since the size of the VSU at the two phases is same, we just need to check that whether the LC class had changed during the period one by one. Thus, the high resolution images at the two phases were compared by changing the timeline of GE. The set of VSUs created for the period 2000–2001 was checked for potential LC changes in the period 2008–2010. For any VSU where a LC change had occurred between 2000–2001 and 2008–2010, the new LC classes are attributed to such VSUs to create the set of VSUs for period 2008–2010.

The method used to collect the VSUs of 2000–2001 (600 m × 600 m) is same to that of the VSUs of 2000–2001 (1 km × 1 km), while they were based on the VSUs of 2000–2001 (1 km × 1 km). Similarly, the method used to collect the VSUs of 2008–2010 (600 m × 600 m) is same to that of the VSUs of 2008–2010 (1 km × 1 km), while they were based on the VSUs of 2000–2001 (600 m × 600 m). The spatial distribution and the number of the VSUs of each LC class are shown in Fig. 2 and Table 5, respectively.

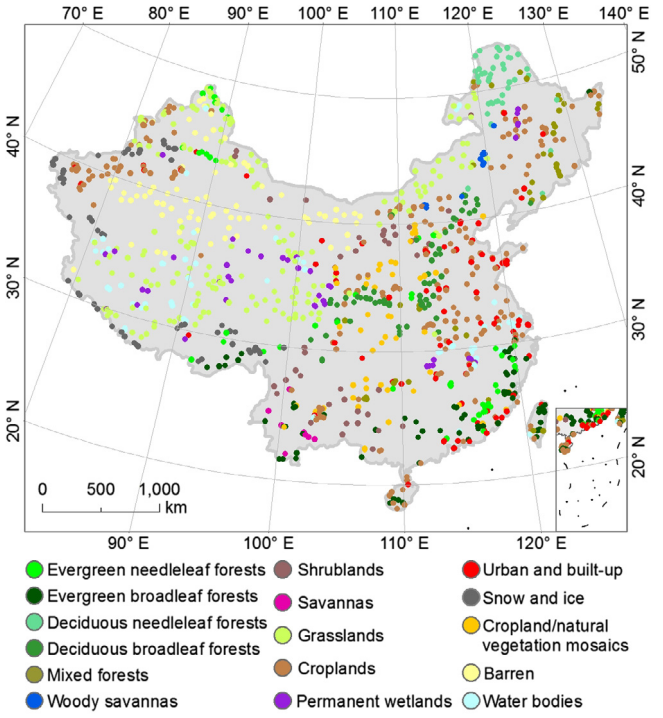

Fig. 2. Spatial distribution of the set of VSUs in 2000–2001 (2 km × 2 km). The spatial distribution of other sets of VSUs are very close to it, since they were all derived from this set directly or indirectly.

Note that GlobeLand30 2010 was assessed using the VSUs of 2008–2010 (600 m × 600), after removing the VSUs of some classes, including cropland/natural vegetation mosaic, woody savannas, and savannas, and the VSUs of five classes of forests were aggregated into forest to match the classes of GlobeLand30 2010. Two different approaches were used for accuracy assessment of GlobeLand30 2010. The first is assessing the GlobeLand30 2010 using the VSUs with size of 600 m × 600 m directly, with an assumption that the VSUs size of 600 m × 600 m is homogeneous, and the classes of all 30-m pixels within the VSUs are the same. The second is assessing the GlobeLand30 2010 after it has been

Table 5
Number of VSUs of each LC class for the accuracy assessment of LC maps.

Class name	IGBP DISCover	UMD	GLC 2000	MCD12Q1 2001	MCD12Q1 2010	GLCNMO 2008	CCI-LC 2000	CCI-LC 2010
Evergreen needleleaf forests	47	47	47	47	47	47	47	47
Evergreen broadleaf forests	70	70	70	70	70	70	70	70
Deciduous needleleaf forests	39	39	39	39	39	39	39	39
Deciduous broadleaf forests	66	66	66	66	66	66	66	66
Mixed forests	41	41	41	41	41	41	41	41
Shrublands	39	39	39	39	40	40	39	40
Woody savannas	11	11	11	11	11	–	11	11
Savannas	8	8	–	8	8	8	8	8
Grasslands	176	176	176	176	176	176	176	176
Permanent wetlands	41	–	41	41	41	41	41	41
Croplands	203	203	203	203	201	201	203	201
Urban and built-up	81	81	81	81	84	84	81	84
Cropland/natural vegetation mosaic	49	–	49	49	47	47	49	47
Snow and ice	57	–	57	57	57	57	57	57
Barren or sparsely vegetation	74	74	74	74	74	74	74	74
Water bodies	61	61	61	61	61	61	61	61
Total	1063	918	1057	1063	1063	1052	1063	1063

resampled to 300-m resolution, so that its pixel size matches that of the VSUs of 2008–2010 (600 m × 600).

2.4. Spatial variation analysis in accuracy

For location (i, j), local spatial accuracy can be computed directly if the validation sample exists there. However, the number of VSUs is always actually far smaller than the number of pixels in the entire study area. For locations with no existing VSU, we defined a geographically weighted statistical approach via Eqs. (3) and (4) to estimate their accuracy. From Eq. (3), the local spatial accuracy is a weighted overall accuracy based on the geographically constrained VSUs. Eq. (4) allows VSUs that are further away from location (i, j) to less affect its accuracy, rather than making an equal contribution.

$$A_{(i,j)} = \frac{\sum_{1}^{N} bW_{k(i,j)}}{\sum_{1}^{N} W_{k(i,j)}} \times 100\% \tag{3}$$

$$W_{k(i,j)} = \begin{cases} \exp(-(d_{k(i,j)}/d)^2), d_{k(i,j)} < d \\ 0, otherwise \end{cases} \tag{4}$$

where $A_{(i,j)}$ is a measure of the local spatial accuracy, $W_{k(i,j)}$ is the contribution that the k-th reference point has to location (i, j), $d_{k(i,j)}$ indicates the distance between the k-th reference point and location (i, j), b is a binary variable, and 1 indicates that the type of the VSU is same to that of the LC map at the k-th point; otherwise b will be assigned as 0. Further, N is the number of VSUs used for local accuracy assessment at location (i, j), and d is a bandwidth or a geographical constraint rule that will be used to select an appropriate subset of VSUs for the local accuracy model. The definition of d will be described in the following.

One concern for local accuracy assessment is defining a suitable geographical constraint rule (Foody, 2005). For local accuracy assessment, in the case that the total number and the spatial distribution of the VSUs are known, the subset of the VSUs used to calculate local accuracy is limited by the size of the searching window or bandwidth. If we hope more VSUs participate in the local accuracy assessment, the only way is to expand the bandwidth. Then, however, the result will be more close to a global assessment rather than a local assessment when the bandwidth is setting too large. Whereas, a false spatial trend originating from the uncertainty of VSU will increase only if a small number of VSUs are used. Furthermore, the bandwidth should change adaptively according to the density of VSUs, e.g., a larger bandwidth is needed in regions with relatively low VSU density than in regions with higher VSU density. In this study, a subset of the VSUs used at location (i, j) was selected as the flowing steps:

Step 1: Generating connected objects using the LC maps. A connected object is a cluster of pixels with the same class at 8-connected direction. The connected object will be used as a searching window to find a subset of VSU used for calculating the local accuracy of (i, j) in step 2. On the Earth surface, the same LC class at a local region has the same or similar spectral characteristics. The classification process is to assign a unique label to each pixel according to its spectral characteristics. I.e. the pixels with same and similar spectral characteristic will be labeled as the same class. In return, we can assume that each connected object corresponds to a homogeneous landscape patch on the Earth's surface. Fig. 3 is a sample illustrating the relationship between landscape patches on Earth's surface and connected objects derived from LC map.

Step 2: Searching the VSUs included in the connected objects that covers location (i, j). For a specific location (i, j), there must be a unique connected object that covers it. The VSUs within that connected object are then considered as the initial set of VSUs for location (i, j). If there is no VSU include in that connected object, go to step 3 directly. If there is only one VSU, it will be used to calculate the local accuracy at (i, j) alone. Otherwise, an optimal set of VSUs would be chose from the initial set of VSUs, since not all the VSUs included that connected object are appropriate for calculating the local accuracy of location (i, j). One typical case occurs in the Tarim Basin, covered by large areas of desert; hence the corresponding connected-object is very large. Local accuracy will be smoothed if all these VSUs are considered. Thus, the leave-one-out cross-validation method proposed by Cleveland (1979) will be used to select an optimal subset of VSUs from the initial set:

$$CV = \frac{1}{N}\sum_{i=1}^{n}\left(Y_{(i,j)} - \hat{Y}_{\neq(i,j)}(d)\right)^2 \tag{5}$$

where N is the number of VSUs covered by bandwidth d, $Y_{(i,j)}$ is the value (LC class label) of VSU at location (i, j), and $\hat{Y}_{\neq(i,j)}$ is the fitted value at location (i, j) with $Y_{(i,j)}$ not included in the computation process. Eq. (5) can then be repeated with the increasing of bandwidth d, to eventually find a lowest CV. The value of d corresponding to the lowest CV is the optimal bandwidth. All VSUs covered by the optimal bandwidth will be used to estimate the local accuracy at location (i, j).

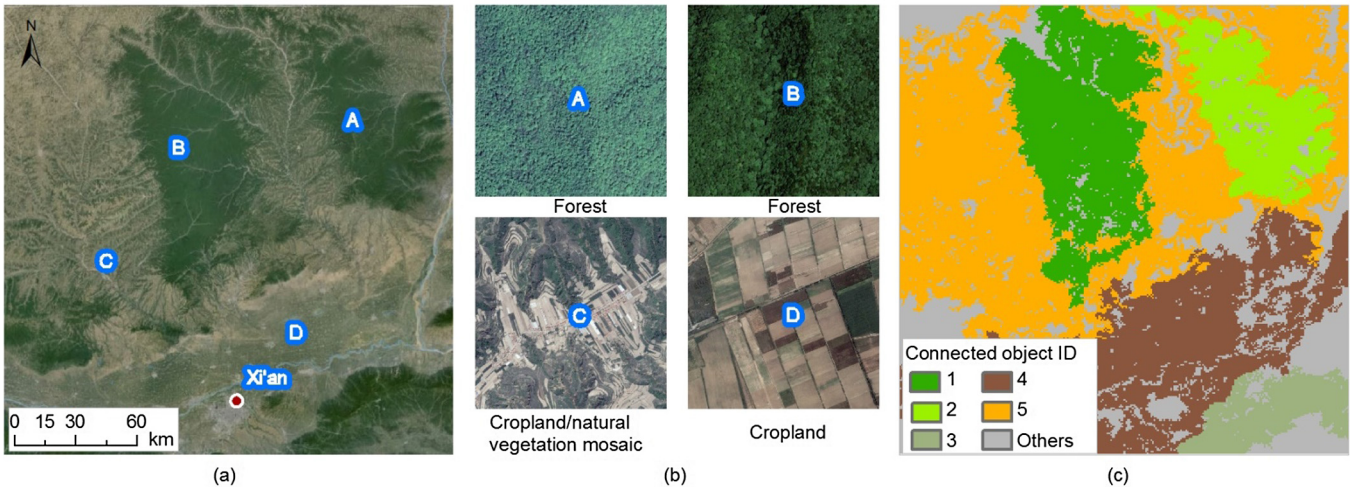

Fig. 3. A sample illustrating the relationship between landscape patches on Earth's surface and connected objects derived from LC map. (a) is a synoptic view of Xi'an and an adjacent region captured from Google Earth; (b) shows the high-resolution images of locations A, B, C, and D, respectively; (c) presents connected objects derived from LC map. The landscape patches on (a) show well one-to-one correspondence with the connected objects on (c).

Step 3: Building an initial testing set using the closest n VSU around location (i, j), if no VSU were found in step 2. It is impractical to ensure that every connected object has one VSU or several VSUs, because of the conflict between the great number of connected objects and the limited number of VSUs. In this study, we selected the closest 150 VSUs as the upper limit of the initial testing set, which is sufficient for the local accuracy assessment (Foody, 2005). Then the optimal bandwidth d and the optimal subset of VSUs were also selected by Eq. (5) automatically.

3. Results

3.1. Areal comparison

We firstly compared the area of five classes of forests of all LC maps except GlobeLand30 2010, since classification scheme adopted in GlobeLand30 2010 does not contain these five classes of forests (Fig. 4). Then, five classes of forests in all LC maps except GlobeLand30 2010 were aggregated into forests, for the purpose making a comparison analysis with GlobeLand30 2010 (Fig. 5).

3.1.1. Five classes of forests

The areas of five classes of forests are very close among GLC 2000, CCI-LC 2000 and 2010. However, they are quite different among the other LC maps. E.g., the area of evergreen needleleaf forests in GLC 2000 is 21.9 times that of MCD12Q1 2001; while the area of mixed forests in MCD12Q1 2001 reaches up 125.5 times that of GLC 2000.

Variances in forest area among the nine LC maps are smaller than that of five classes of forest as expected. E.g., forest areas are very close among GLC 2000, CCI-LC 2000 and 2010, and GlobeLand30 2010. While they still differ greatly among the other maps. The largest forest area found in GLCNMO 2008 is as large as 3.2 times of the smallest found in UMD.

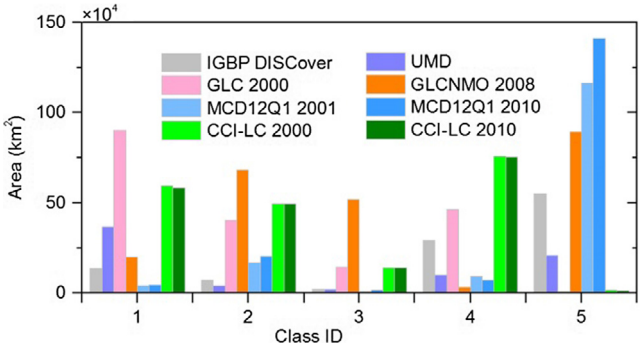

Fig. 4. Area comparison of the five classes of forest among the eight LC maps except for GlobeLand30 2010. Class ID 1 is the evergreen needleleaf forests, 2 is the evergreen broadleaf forests, 3 is the deciduous needleleaf forests, 4 is the broadleaf forests, 5 is the mixed forests.

3.1.2. Shrublands

Shrublands areas in CCI-LC 2000 and 2010, MCD12Q1 2010 and GlobeLand30 2010 are very close, while they are far smaller than that of IGBP DISCover and UMD. Moreover, discrepancy in shrublands areas shows well relationship with the classification scheme used in LC maps. E.g., shrublands area in maps using IGBP scheme (IGBP DISCover, UMD, and MCD12Q1 2001 and 2010) are all greater than maps using LCCS scheme (GLC 2000, CCI-LC 2000 and 2010, GLCNMO 2008, and GlobCover 2009). It can be illustrated by the differences in the definitions of shrublands in the different LC maps. The threshold of shrub canopy is 10–100% in IGBP DISCover, UMD, MCD12Q1, while it is 15–100% in GLC 2000 and CCI-LC, and 40–100% in GLCNMO 2008. Unsurprisingly, LC maps with a wider range of shrub canopy threshold will have more shrublands.

3.1.3. Savannas

The areas of savannas were only compared among IGBP DISCover, UMD, MCD12Q1 2001 and 2010, GLCNMO2008, and CCI-LC 2000 and 2010, as there is no matching class in GLC 2000 and GlobeLand30 2010. Savanna areas are quite small in all LC maps except UMD. E.g., savanna area in UMD is 28 times that of MCD12Q1 2001, and 22 times that of IGBP DISCover. The overestimation of savannas in UMD depends strongly on the over-sampling of the training site used to identify savannas. During the UMD development process, savannas, as typical tropical landscapes, have training databases not only in tropical regions but also in temperate and boreal zones (Hansen et al., 2000).

3.1.4. Urban and built-up

As expected, GlobeLand30 2010 has the largest area of urban and built-up, since small towns and villages can be captured on

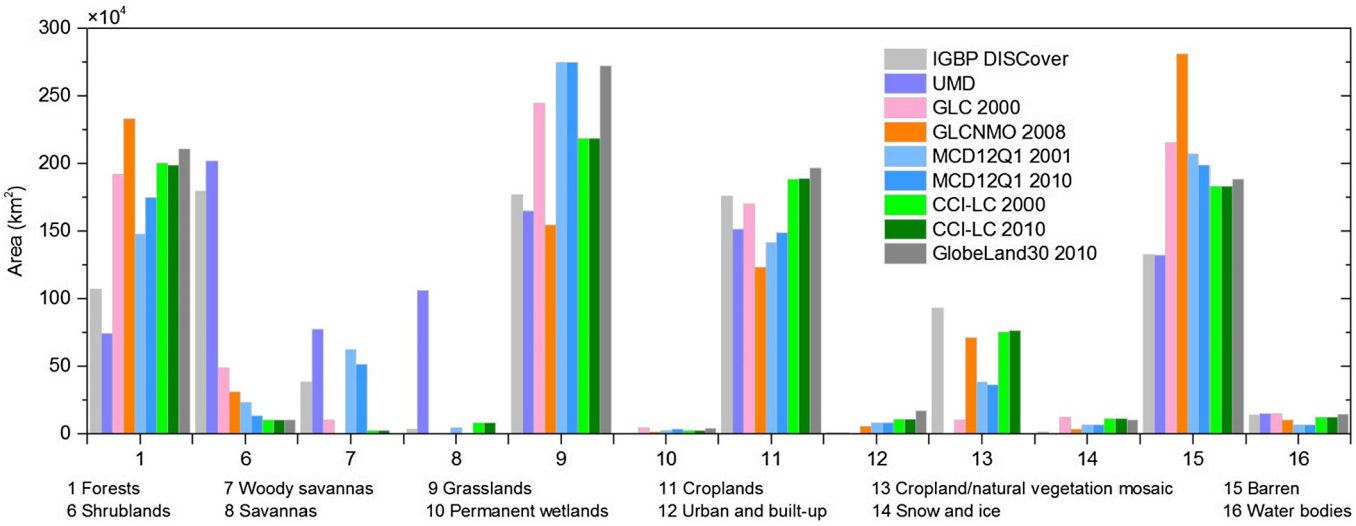

Fig. 5. Area comparison of LC classes among the nine LC maps. Excluding GlobeLand30 2010, five classes of forest (evergreen needleleaf forests, evergreen broadleaf forests, deciduous needleleaf forests, deciduous broadleaf forests, and mixed forests) in the other eight LC maps were aggregated into forests.

30-m resolution images (i.e. TM, ETM+, and HJ-1), while they will be lost in coarse resolution images (i.e. AVHRR, MODIS, SPOT VEGETATION, and ENVISAT MERIS). In addition, although the areas of urban and built-up in CCI-LC and MCD12Q1 are similar to that of GlobeLand30 2010, they both lose the ability to reflect the urbanization process in China during the period from 2000 to 2010. E.g., urban area of MCD12Q1 2001 (82,276 km^2) is even greater than that of MCD12Q1 2010 (82,244 km^2), while urban area of CCI-LC 2000 is identical to that of CCI-LC 2010. Besides, urban area in GLC 2000 is even far smaller than those in IGBP DISCover and UMD. However, urban area should increase continuously from 1992 to 2010 owing to the rapid urbanization process.

These unreasonable phenomena depend strongly on the classification method to extract urban in different LC maps. Urban and built-up, as class with small spatial extents and patch size, will not be well presented on coarse resolution satellite images. Method used to extract urban and built-up are very different in the nine maps. E.g., urban in CCI-LC came from the global urban map produced by Schneider et al. (2010) using 500-m MODIS data in 2001–2002 (Defourny et al., 2016), thus it must results in an underestimation of urban in 2010. Urban in MCD12Q1 2001 and 2010 was obtained based on same training sites centered on 2001–2002 (Schneider et al., 2009; Friedl et al., 2010), these outdate training sites must lead to an under-sampling of urban in 2010, as well as the under-mapping of urban in 2010. Urban in GLC 2000 was extracted using visual interpretation method (Xu et al., 2005), small patches of urban may be ignored unconsciously and thus results in its underestimated. Additionally, the outdated urban layer from the Defense Mapping Agency data (DMA, 1992) may have led to its underestimation in IGBP DISCover and UMD (Loveland et al., 2000). As urban layer in DMA was drawn from maps produced in the 1960–1980s, it is too dated to represent urban areas of China due to rapid urbanization (Danko, 1992). In GLCNMO 2008, urban was mapped mainly using population data, constructed imperious surface area data, DMSP OLS nighttime light data, and MODIS NDVI data, and four thresholds corresponding to these four data was built to extract urban step by step. Naturally, uncertainty in the four thresholds can largely affect the result.

3.1.5. Barren

Barren areas are relatively similar in all LC maps except GLCNMO 2008, IGBP DISCover, and UMD. The largest barren area found in GLCNMO 2008 has direct relation with the definition of vegetation canopy threshold of barren. In GLCNMO 2008, the threshold of vegetation canopy for barren is <40%, which is quite wider than that of other LC maps, i.e. <10% and 15%. The smallest barren areas found in IGBP DISCover and UMD is closely related to the over-mapping of shrublands. As shown in Fig. 6, there are large areas of shrublands in arid or semi-arid regions in IGBP DISCover and UMD, where the main LC class should be barren actually.

3.1.6. Water bodies

Unexpected, the largest water area is found in GLC2000; and water areas in other two 1-km LC maps (IGBP DISCover and UMD) are also greater than that of 300-m or 500-m LC maps. More exaggerated, water area in MCD12Q1 is even smaller than half of that in IGBP DISCover, UMD, and GLC 2000. In general, more water will be observed when the resolution of satellite images was improved from 1 km to 30 m. Since the patch size of inland water is often smaller than the pixel size of satellite images, it will not be well present on coarse resolution images. The under-mapping of water in MCD12Q1 has directly relation with its classification method. Water in MCD12Q1 was classified by supervised classification method together with other classes (Friedl et al., 2010). However, as a class with small spatial extent and patch size, it will not be well presented when classified together with other classes using coarse satellite data. The over-mapping of water in GLC 2000 is close related to the overestimation of the lakes in Mid-Lower Reaches of Yangtze River. It should be noticed that water in CCI-LC was extracted using 150-m resolution ASAR data instead of optical images.

3.2. Visual comparison

Fig. 6 shows the spatial patterns of LC classes among nine LC maps. Overall, the general spatial patterns of all classes over China viewed at national scale are obvious. However, it cannot dissimulate the evident difference in the spatial distributions of some classes in local regions, such as five classes of forests, shrublands, and grasslands.

3.2.1. Five classes of forests

The overall spatial patterns of the five classes of forests in GLC 2000, CCI-LC 2000 and 2010 fit well the actual distribution of forests in China; except that deciduous broadleaf forests found in Changbai Mountains were obvious overestimated in these three

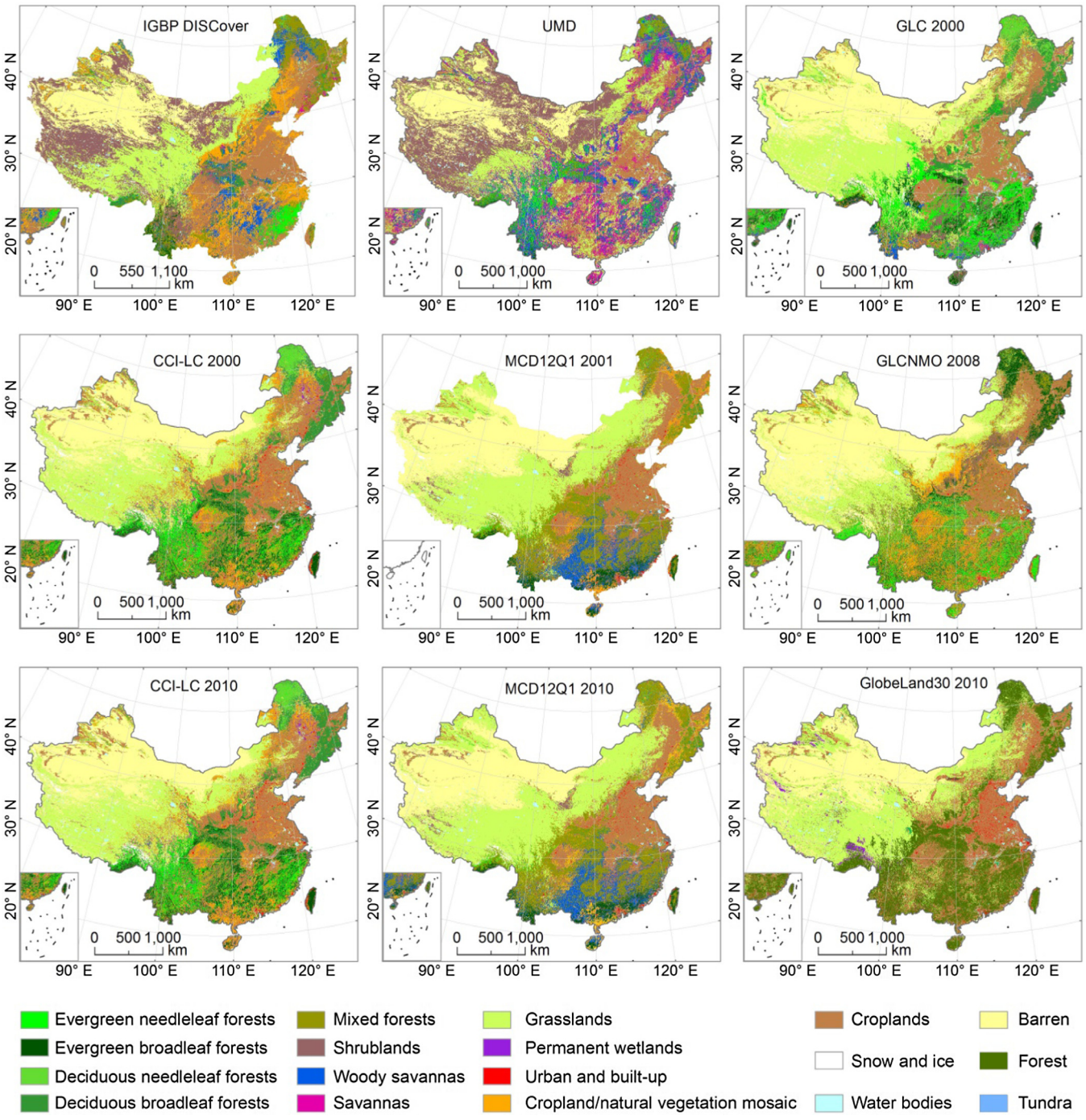

Fig. 6. Spatial patterns of LC classes in IGBP scheme for the nine LC maps.

LC maps, where the domain LC class should be mixed forests actually.

However, the spatial patterns of five classes of forests in other maps are very different. E.g., mixed forests are widely distributed in mountain areas of China in MCD12Q1 2001 and 2010; while they are very rare in CCI-LC 2000 and 2010, GLC 2000, and GLCNMO 2008. GLCNMO 2008 even has large areas of evergreen broadleaf forests in Da Hinggan Ling and Xiao Hinggan Ling, and Changbai Mountains. In fact, evergreen broadleaf forests mainly occur in Southeast Hills, Taiwan, and Hainan. Large areas of evergreen needleleaf forests mainly occur in high-cold mountain (e.g. Hengduan Mountains, Tianshan Mountains, and mountain area in western Sichuan); and some mountains and hills in Zhejiang, Fujian and Jiangxi Province. While, large areas of mixed forests occur in Xiao Hinggan Ling and Changbai Mountains.

3.2.2. Shrublands

Shrublands are widely distributed in arid or semi-arid region of China in IGBP DISCover and UMD. E.g., large areas of shrubland can be found in Xinjiang, Gansu, Inner Mongolia, and Xizang Province. However, the distributions of shrublands in other seven maps are very rare and scattered.

3.2.3. Savannas

As expected, the spatial distribution of savannas in UMD is much wider than that of other LC maps. As described above, savan-

nas in UMD are largely overestimated because UMD has many training samples in temperate and boreal zones. In China, however, savannas can only be found in the dry and hot valleys in Yunnan Province.

3.2.4. Grasslands

Although general patterns of grasslands are similar among the nine LC maps, some obvious differences can still be found in several local regions. E.g., IGBP DISCover, MCD12Q1 2001 and 2010, and GlobeLand30 2010 have more grasslands in the northeast part of Inner Mongolia and the northern transition zone than GLC 2000, CCI-LC 2000 and 2010. While, IGBP DISCover, UMD, MCD12Q1 2001 and 2010, and GLCNMO 2008 have less grasslands in the northern Tibetan Plateau than GLC 2000, CCI-LC 2000 and 2010, and GlobeLand30 2010.

3.2.5. Barren

Although the barren class in all LC maps occurs in arid or semi-arid region in China, they are still quite different in some local regions. Obvious difference can be found in the northeast part of Inner Mongolia Plateau and north part of Tibet Plateau. In Inner Mongolia, barren areas in GCL 2000, CCI-LC 2000 and 2010 are far greater than that of MCD12Q1 2001 and 2010, and GlobeLand30 2010. While, in north Tibet Plateau, barren areas in MCD12Q1 2001 and 2010, and GLCNMO 2008 are well greater than that of CCI-LC 2000 and 2010, GLC 2000, and GlobeLand30 2010.

3.3. Per-pixel comparisons

Per-pixel comparison was initially conducted among maps at close year. In order to analyse consistency of maps at different year but from the same institutes, per-pixel comparison was also done between MCD12Q1 2001 and MCD12Q1 2010, as well as CCI-LC 2000 and CCI-LC 2010. Moreover, considering that GlobeLand30 2010 should have higher accuracy than other LC maps with coarse resolution, due to its higher resolution and improved mapping technique (POK-based). It is interest to analyse which LC map best fit GlobeLand30. Thus per-comparison between GlobeLand30 2010 and other LC maps were also performed.

Table 6
Resampling method adopted in LC maps.

LC map	Target resolution (m)	Resample method
MCD12Q1 2001, 2010 (500 m)	1000	Nearest neighbor rule
GLCNMO 2008 (500 m)	500, 1000	Nearest neighbor rule
CCI-LC 2000, 2010 (500 m)	500, 1000	Nearest neighbor rule
GlobeLand30 2010 (30 m)	300, 500, 1000	Majority rule

Since the nine maps range in resolution from 30 m to 1 km, Resampling is needed for comparison analysis. Resampling strategy is not exactly same for different comparing group. E.g., CCI-LC 2000 was resampled to 1 km when compared with GLC 2000, while resampled to 500 m when compared with MCD12Q1 2001. Resampling methods used for different maps are also different (Table 6). Nearest neighbor rule was used for map whose resolution is relatively close (300 m, 500 m, and 1 km). While, majority resampling was used to resample GlobeLand30 2010 to 300 m, 500 m, and 1 km, respectively, as the huge gap from 30 m to 300 m and 500 m makes it is inappropriate using nearest neighbor rule.

The overall spatial agreement between LC maps produced by different institutes is relatively low (Table 7). The highest overall spatial agreement found between GLC 2000 and CCI-LC 2000 is 53.8%. This has a certain relationship to one fact that GLC 2000 was one of the dozens of alternative global or regional reference maps used to define training maps for CCI-LC. It was used when no other reference maps were considered to be better suited for reference map. The secondary is found between GLCNMO 2008 and MCD12Q1 2010 (50.3%). The overall spatial agreement indexes between other LC maps are all lower than 50%. E.g., the lowest agreement found between IGBP DISCover and UMD only accounts for 39.4% of the lfand area of China. The overall spatial agreement between CCI-LC 2000 and 2010 is as high as 99.8%. However, this does not mean that there is only 0.2% LC has changed from 2000 to 2010. In fact, for the current released version of CCI-LC, only forest dynamics have been detected and mapped, the other classes in CCI-LC 2000 are identical to CCI-LC 2010 (Defourny et al., 2016).

The overall spatial agreement between MCD12Q1 2001 and 2010 is 73.2%. While individual-class spatial agreement of five classes of forests, permanent wetlands, croplands, and urban and built-up are very low between MCD12Q1 2001 and 2010, even similar training database and classification technique were used to produce these two LC maps (Friedl et al., 2010). Moreover, although urban layer used in MCD12Q1 2001 is same to that of MCD12Q1 2010, their spatial agreement is only 61.8%. This issue was caused by new spatial error introduced through the re-projection process. For the urban and built-up, as a class with small spatial extent and patch size, a slight spatial displacement can significantly reduce its spatial agreement between different LC maps.

Fig. 7 presents the spatial agreements and disagreement between different LC maps. The high spatial agreements mainly occur in homogeneous regions, e.g. regions covered by large areas of barren, grasslands, and croplands, such as the North China Plain and Tarim Basin. However, the low spatial agreements are widely distributed in heterogeneous regions, e.g. regions covered by cropland/natural vegetation mosaic, and different classes of forests, such as Yunnan-Guizhou Plateau, Southeast Hill, and most parts of mountains in China. However, one exception is that the spatial

Table 7
Overall spatial agreement (A_O) (%) and individual-class spatial agreement (A_i) (%) among different LC maps.

LC maps	A_O	A_1	A_2	A_3	A_4	A_5	A_6	A_7	A_8	A_9	A_{10}	A_{11}	A_{12}	A_{13}	A_{14}	A_{15}	A_{16}
IGBP DISCover and UMD	39.4	9.3	12.7	14.5	10.7	29.3	49.4	13.6	1.5	41.4	0	50.6	26.2	0	0	63.8	46.2
MCD12Q1 2001 and GLC 2000	47.8	3.1	16.6	8.5	22.0	1.2	3.0	6.1	0.0	60.3	1.7	59.7	7.3	3.8	45.8	77.2	37.3
MCD12Q1 2001 and CCI-LC 2000	47.5	7.7	26.8	9.7	16.6	1.8	0.2	0.5	0.8	59.8	1.0	58.0	35.3	12.0	57.6	78.1	57.8
GLC 2000 and CCI-LC 2000	53.8	30.8	32.6	63.2	49.1	3.8	7.4	0.2	0.0	60.6	4.0	58.6	8.4	4.7	56.0	78.6	49.1
MCD12Q1 2010 and CCI-LC 2010	49.3	7.4	27.2	14.7	15.2	1.5	0.2	0.4	0.2	62.3	3.3	62.7	37.1	14.5	61.8	78.5	58.0
MCD12Q1 2010 and GLCNMO 2008	50.3	0.8	7.6	0.3	0.1	25.5	4.1	0.0	0.0	59.4	3.1	67.5	47.1	11.9	59.2	79.5	64.9
CCI-LC 2010 and GLCNMO 2008	42.0	9.7	17.2	1.1	0.3	1.6	1.0	0.0	0.0	47.2	0.8	56.7	40.2	22.5	46.3	72.6	73.9
CCI-LC 2000 and 2010	99.8	99.3	99.9	99.9	99.8	85.3	100.0	100.0	100.0	100.0	100.0	100.0	100.0	100.0	100.0	100.0	100.0
MCD12Q1 2001 and 2010	73.2	23.8	62.2	12.0	33.2	66.9	19.9	44.8	0.7	83.1	12.8	72.1	61.8	32.9	71.2	90.9	79.0

agreements of five classes of forests are very well between CCI-LC 2000 and GLC 2000.

Table 8 shows overall and individual-class spatial agreement between GlobeLand30 2010 and other six LC maps. Among all the six maps, MCD12Q1 2010 has the highest overall agreement (67.7%) with GlobeLand30 2010, which is slightly larger than that of CCI-LC 2010 and GCL 2000, which are 64.1% and 62.1%, respectively. For the individual class, highest spatial agreements of forests, permanent wetlands, and water bodies are both found between CCI-LC 2010 and GlobeLand30 2010. While the highest spatial agreement of grasslands, croplands, snow and ice, and barren are found between MCD12Q1 2010 and GlobeLand30 2010.

3.4. Comparison of validation results

Nine confusion matrices of each LC map were established based on the five sets of VSUs; however, they were shown as supplementary material limited by the length of the paper. Four accuracy measures (i.e. overall accuracy, user's and producer's accuracy, Kappa coefficients) were derived from these confusion matrices.

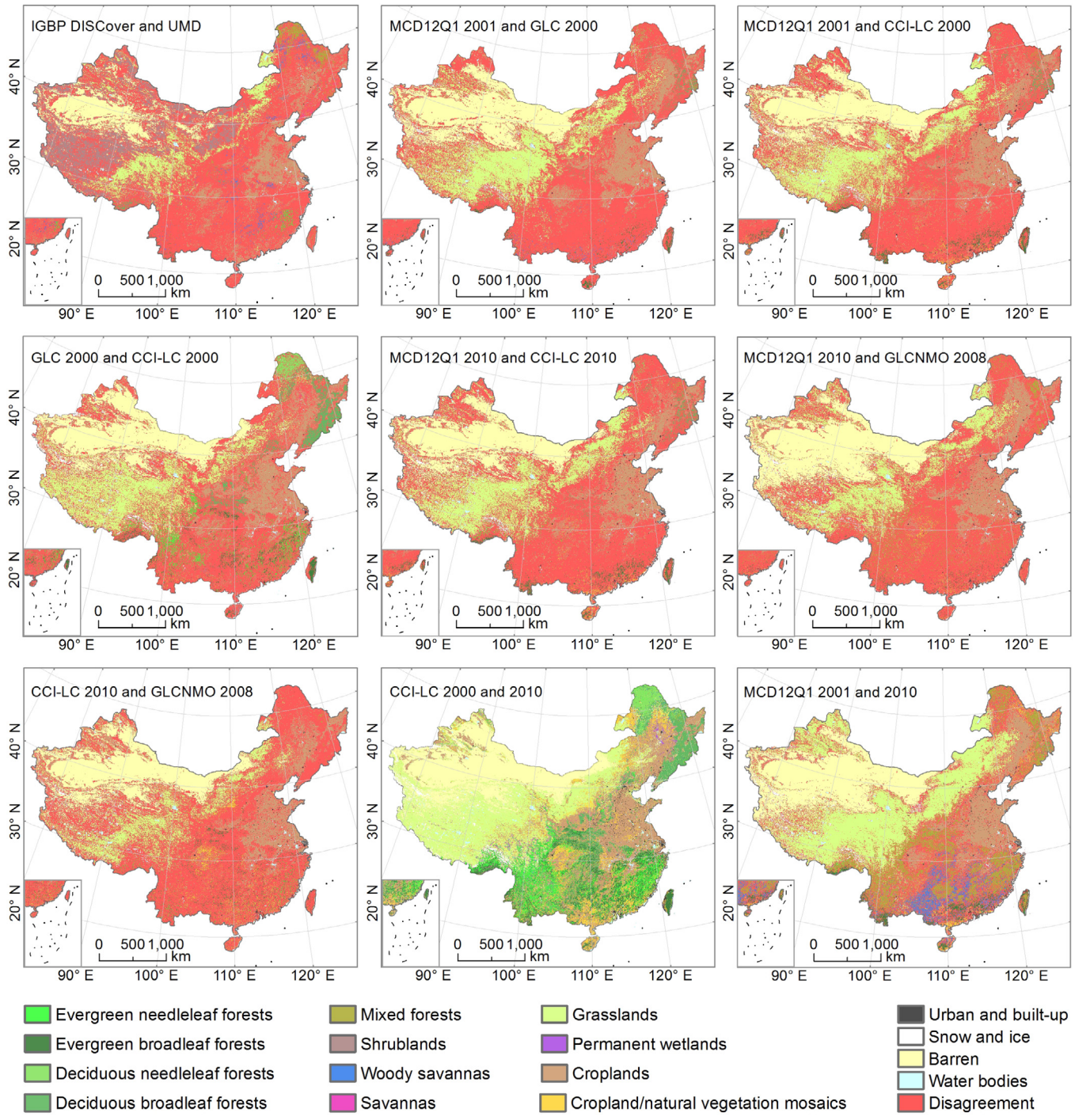

Fig. 7. Spatial agreement and disagreement between different LC maps. Pixels with the same class in both two different LC maps will retain their values, and the color system used for agreement pixels is same to that of Fig. 5; otherwise will be labeled as disagreement.

Table 8
Overall spatial agreement (A_O) (%) and individual-class spatial agreement (A_i) (%) between GlobeLand30 2010 and the six LC maps.

LC map	A_O	Forests	Shrublands	Grasslands	Permanent wetlands	Croplands	Urban and built-up	Snow and ice	Barren	Water bodies
IGBP DISCover	45.8	47.5	3.1	55.0	0.0	53.6	3.6	12.3	70.8	32.1
UMD	35.5	40.1	2.7	35.5	0.1	46.8	3.4	0.0	62.5	31.0
GLC2000	62.1	66.2	2.2	61.0	6.2	60.1	3.8	47.3	78.2	36.9
GLCNMO2008	59.7	71.5	2.1	51.4	5.1	57.0	31.6	44.4	74.6	57.0
MCD12Q1 2010	67.7	74.6	1.8	70.1	4.7	64.9	30.3	59.1	82.2	53.3
CCI-LC 2010	64.1	75.6	0.5	61.7	12.3	61.1	28.6	58.8	78.4	61.2

Since the classification scheme used in GlobeLand30 is different from that of the other eight LC maps, it is difficult to compare their accuracy directly. Thus, we also calculated the accuracy of the eight LC maps based on an aggregated classification scheme (i.e. forests, shrublands, grasslands, permanent wetlands, croplands, urban and built-up, snow and ice, barren, and water bodies).

Excluding GlobeLand30 2010, CCI-LC has the highest overall accuracy (Table 9). Low overall accuracy of IGBP DISCover, UMD, and GLC2000 obtained here is not surprise, and the accuracy obtained here well agree with that provided by Ran et al. (2010). The overall accuracy provided by Ran et al. (2010) for IGBP DISCover, UMD, and GLC2000 over China was 57.09%, 54.17%, and 59.28%, respectively. However, they were evaluated upon a scheme contains seven classes (i.e. croplands, wetlands, urban, forest/-woodlands, grass/shrubland, barren/ice, and water bodies). Naturally, the accuracy will decrease sharply when they were estimated based on scheme contains more classes. The overall accuracy of GlobeLand30 2010 is 82.39% when it was evaluated using the VSUs of 2008–2010 (600 m × 600 m) directly; while it is 82.07% after it has been resampled to 300-m resolution by majority resample rule, which is slightly lower than the former. As the VSUs were selected in areas where the classes of the four pixels are the same, this will have clearly a bias (higher accuracies) as most heterogeneous areas at 30 m resolution will be not considered. That's also why the result obtained in this study from two validation methods used for this LC map (without or with resampling at 300 m) are very similar. Note that the overall accuracies of GlobeLand30 2010 gained by these two methods are all greater than its global overall accuracy (80.30%) provided by Chen et al. (2014).

One interesting case is that the overall accuracy of GLC 2000 (50.14%) is even greater than that of GLCNMO 2008 (48.76%). In general, mapping accuracy will increase as the improvement of the spatial resolution. However, this relation is not absolute. Since the resolution is just one of the many factors that affect the classification accuracy. Further, the classification strategy and method also have huge influence to the accuracy. GLC 2000 was produced by JRC in partnership with 30 institutes (Bartalev et al., 2003; Stibig et al. 2004; Mayaux et al., 2006). The LC map in China, as part of GLC2000, was produced by Institute of Remote Sensing Applications of Chinese Academy of Science (Xu et al., 2005) using unsupervised method (ISODATA). The whole territory of China was stratified into nine homogeneous bio-climatic regions based on climate condition. Data pre-processing, classification, interpreting, and labeling process were carried out for each regions separately. By this way the spectral difference for same LC class at different regions will reduce significantly. Besides, the interpreting and labeling of the cluster result was based on both 1:1,000,000 land use map of China (1990) and 1:1,000,000 vegetation map of China (2000). As a result, the classification result will better fit the real condition of China. GLCNMO 2008 was produced using supervised method except urban, snow and ice, water, and wetland. However, training samples in China are very rare and only center on limited regions. As a result, these training samples must provide poor representation of the LC classes in China, and the low accuracy found in China is not a surprise.

Table 9
Overall accuracy and Kappa coefficient for the nine LC maps.

LC map	Overall accuracy (%)		Kappa coefficient	
	IGBP scheme	Aggregated scheme	IGBP scheme	Aggregated scheme
IGBP DISCover	37.44	44.34	0.30	0.36
UMD	31.86	38.46	0.24	0.29
GLC 2000	50.14	59.35	0.44	0.52
GLCNMO 2008	48.76	58.04	0.44	0.51
CCI-LC 2000	58.54	71.87	0.54	0.64
CCI-LC 2010	58.65	71.98	0.54	0.65
MCD12Q1 2000	55.88	70.23	0.51	0.64
MCD12Q1 2010	56.04	70.37	0.51	0.64
GlobeLand30 2010	–	82.39	–	0.78

Classes with high user's accuracy but low producer's accuracy indicate an under-mapping (Fig. 8). One typical case is urban and built-up in IGBP DISCover, UMD, and GLC 2000. The low producer's accuracies (18.83%, 13.58%, and 8.64% for IGBP DISCover, UMD, and GLC 2000, respectively) indicate that large areas of urban and built-up on the ground are not committed to this class. The confusion matrix highlights that abundant areas of urban and built-up are misclassified into croplands. On the contrary, Classes with high producer's accuracy but low user's accuracy imply an over-mapping. One case is barren in GLCNMO 2008, in which producer's and user's accuracies are 92.57% and 42.47%, respectively. The confusion matrix shows that this commission is mainly caused by misclassification with grasslands. In addition, the highest producer's accuracy of savannas, which occurs in the UMD map, was also achieved at the cost of serious overestimation. Finally, classes with both low user's accuracy and low producer's accuracy indicate that they are quite low-accurately mapped, such as shrublands, permanent wetlands, woody savannas, and savannas. E.g., wetlands represent a condition of LC consisting of configurations of water, trees, or herbaceous cover; thus, lands covered with forests or herbaceous vegetation on regularly flooded or waterlogged soil are easily misclassified into forest and grasslands.

Fig. 9 shows the user's and producer's accuracy of the five classes of forests in the eight LC maps with coarse resolution. Neither of the LC maps has both high user's and producer's accuracy. The relatively high producer's accuracy and low user's accuracy of mixed forests, found in MCD12Q1 2001 and 2010, well explains the over-mapping of mixed forests in these two maps. Besides, the low user's accuracy and relatively high producer's accuracy of deciduous broadleaf forests, found in CCI-LC 2000 and 2010, also illustrates its over-mapping in these two maps.

3.5. Spatial variation in accuracy

Spatial analysis in classification error was performed in six LC maps (IGBP DISCover, UMD, GLC 2000, GLCNMO 2008, CCI-LC 2010, and MCD12Q1 2010) based on IGBP scheme (Fig. 10). In case that CCI-LC 2000 and CCI-LC 2010 show extremely high spatial

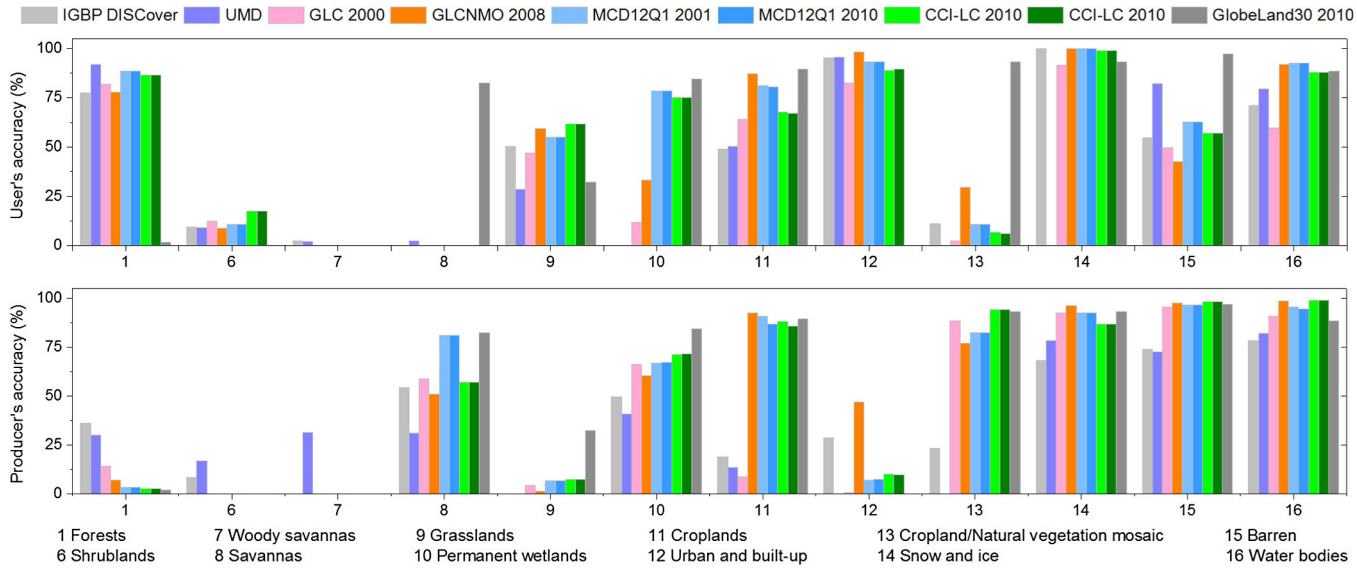

Fig. 8. Comparison of the user's and producer's accuracy of LC classes among the nine LC maps.

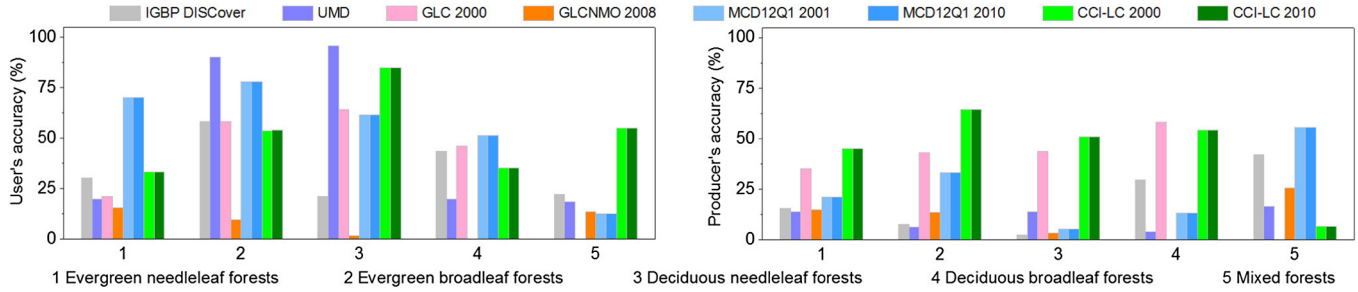

Fig. 9. Comparison of the user's and producer's accuracies of the five classes of forest among the eight LC maps except for GlobeLand30 2010.

agreement, there is no need to conduct spatial analysis for both of them. Only CCI-LC 2010 was considered here because its overall accuracy is slightly greater than that of CCI-LC 2000. For the same reason, MCD12Q1 2010 was considered from the two LC maps of MCD12Q1 dataset. Due to the high spatial resolution, the size of GlobeLand30 2010 is too large to conduct spatial analysis, thus it is not involved too.

Local accuracy derived from the geographically weighted statistical approach varies markedly across the study area. With the overall accuracies of the six LC maps ranging from 31.86% to 58.65%, their local accuracy can span the entire range from 0% to 100%. Fig. 10 depicts the spatial variation in classification accuracy of the six LC maps.

In general, local accuracy has apparent relationship with the degree of landscape heterogeneity. On one hand, the six LC maps all show high local accuracy in regions with relatively low landscape complexity, e.g. the Tarim Basin and North China Plain. On the other hand, they all show low local accuracy in regions with high landscape complexity, e.g. mountainous areas or hilly regions of China. Thus, it is not surprise that landscape heterogeneity has been regarded as a major factor driving LC mapping accuracy (Herold et al., 2008; van Oort et al., 2004). Landscape heterogeneity can significantly complicate the spectral characteristics of the Earth's surface, and thus LC mapping is becoming difficult.

However, there are also some regions where local accuracies in the six LC maps are quite different. Such as Da Hinggan Ling, Sichuan Basin, Northern Tibetan Plateau, and Southeast Hills of China.

In Da Hinggan Ling, the local accuracy is very high in GLC 2000 and CCI-LC 2010, while it is very low in other four maps. In fact, deciduous needleleaf forests, constitutes the prime LC class here, were largely misclassified into mixed forest in IGBP DISCover, UMD, and MCD12Q1 2010, and mislabeled as evergreen broadleaf forest in GLCNMO 2008.

In Sichuan Basin, all LC maps present low local accuracy except GLCNMO 2008 and CCI-LC 2010. The domain LC type is croplands/-natural vegetation mosaic composed of terraced field and forest, however, large areas of cropland/natural vegetation mosaic were labeled as croplands in IGBP DISCover, UMD, GLC 2000, and MCD12Q1 2010.

In the Northern Tibetan Plateau, GLC 2000 and CCI-LC 2010 show high local accuracy, while the other four maps all show low local accuracy. Grassland, as the prime LC class here, were seriously misclassified into shrubland in IGBP DISCover, UMD, and MCD12Q1 2001, but was misclassified as barren for GLCNMO 2008 and MCD12Q1 2010.

In Southeast Hills of China, the local accuracy in GLCNMO 2008 and CCI-LC 2010 are relatively higher than other four maps. The landscape in Southeast Hills of China is very complex, where land surface is covered by evergreen broadleaf forests, evergreen needleleaf forests, croplands, and mosaic. E.g., MCD12Q1 2010 has large areas of woody savannas, which was result from the misclassification with cropland/natural vegetation mosaic.

Inevitably, the spatial analysis results of the classification accuracy will contain uncertainties. First, if there is only a few VSUs (perhaps only one VSU) in a large connected object, the accuracy

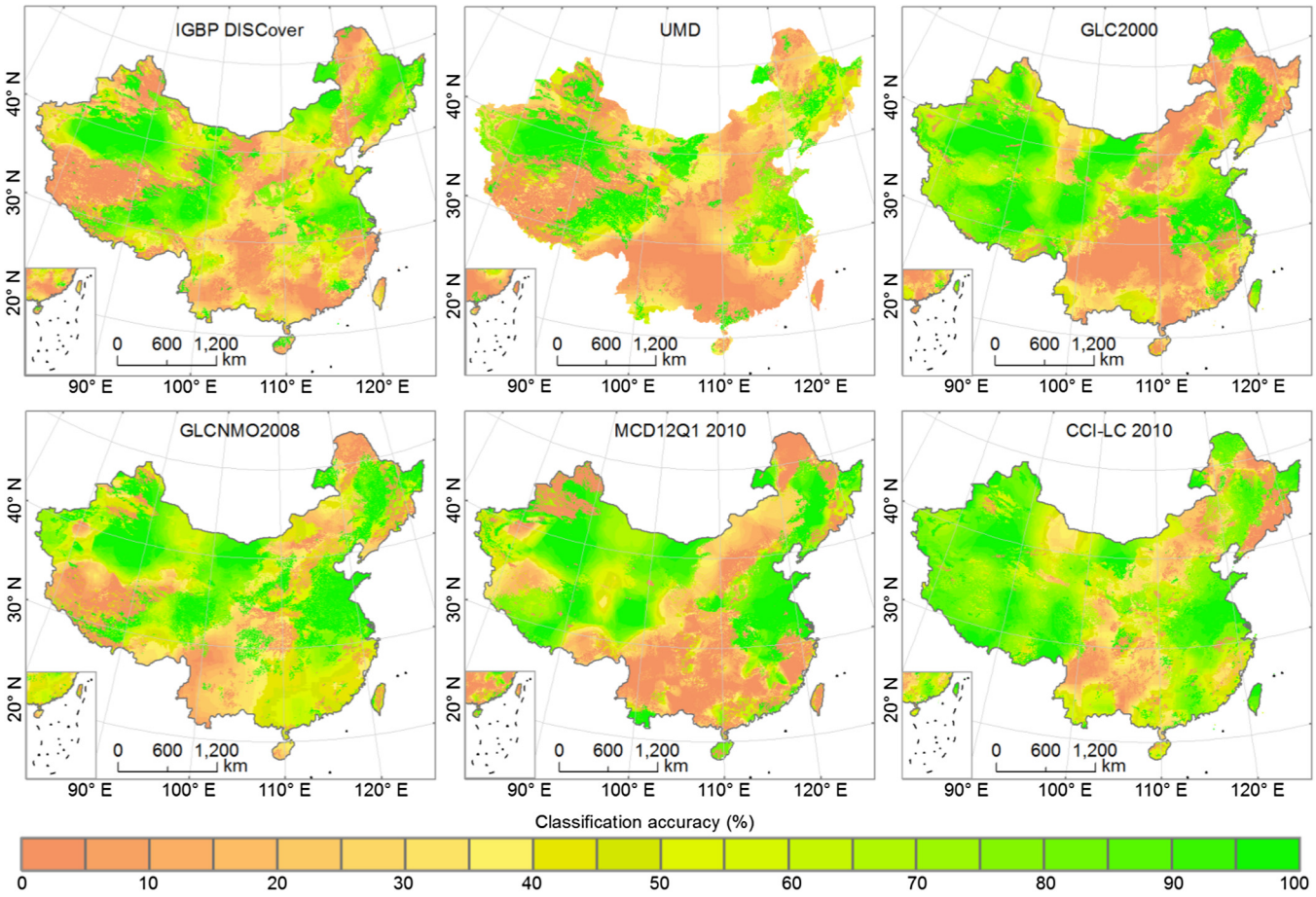

Fig. 10. Visualization of the spatial variation in classification accuracy for the six LC maps. Unlike a single global estimate of classification accuracy, local accuracy is a sub-region estimate obtained by geographically constraining the VSUs used for accuracy assessment.

of some pixels covered by the connected object will be overestimated, while the accuracy of the other pixels will be underestimated. Second, when the VSUs used at each target pixel were selected by the bandwidth, then bandwidth in regions with low sample density must be greater than that with high sample density. With increasing bandwidth, the representativeness of the VSUs will be sharply reduced; thus, estimating bias will increase. For instance, the actual local accuracy for the Yunnan-Guizhou Plateau and Southeast Hills of China may not be as low as Fig. 10 indicates.

4. Discussion

For future global LC mapping, more attentions should be paid to the experiences and lessons from previous global LC mapping activities. Several aspects which deserve of further research in the future are summarized below.

4.1. Issues related to classification scheme

Difference in classification schemes is one of the major factors driving disagreement in classification results. It also makes rigorous comparison and synergistic use of different maps challenging if not impossible (Herold et al., 2008; Gong et al., 2013; Congalton et al., 2014). In addition, for the purpose of comparing and using maps with different schemes, maps with more detailed classes are often transformed into generalized scheme with fewer classes, it will naturally led to the loss of the ability describing detail LC characteristics.

Hence, one emerging thing is the determination of some essential LC classes, if it's impractical to design a universal classification scheme given the similar but not identical application goals of different maps (Gong et al., 2016). On one hand, what we need to do is confirm the classes that are necessary for global LC mapping and can be detected on satellite images. E.g., except the common classes in these maps, it is needed to map class like (1) irrigated croplands and rainfed croplands rather than croplands, (2) evergreen shrublands and deciduous shrublands rather than shrublands, and (3) different kinds of wetlands covered by tree, shrub, or herbaceous separately. Since their ecological functions and their interaction mechanisms with climate are quite different. More importantly, these classes have been proved available at global scale with the improvement of the spatial and temporal resolution of satellite images (Arino et al., 2008; Bontemps et al., 2010; Gong et al., 2013; Defourny et al., 2016). On the other hand, further research should aim to derive a unique LC class definition, especially for essential classes. The second is to decrease the ambiguities in definition of same LC class, in particular the threshold of vegetation canopy of class like forests, grasslands, and shrublands. E.g., the differences of vegetation canopy threshold of shrublands and grasslands can directly influence the classification results, especially in arid or semi-arid regions.

4.2. New thoughts on global mapping of key LC classes

The results presented in the study, as well as those found in previous activities (Hansen and Reed, 2000; Fritz and See 2008; McCallum et al. 2006; Friedl et al., 2010), have demonstrated that

several key classes are problematic and difficult to map. In particular, the low accuracies found in urban and built-up, permanent wetlands, and five classes of forests, are always not satisfying.

Given the small patch size and high internal heterogeneity, mapping of urban and built-up using satellite images is full of challenges. By the way, building urban map separately from other classes, the accuracy of urban in recently released global LC datasets (MCD12Q1, CCI-LC, GlobeLand30) have clear improvement, while they still fail in providing dynamic information on urban change. In recent years, urban mapping using DMSP OLS nighttime light data becomes a booming topic, it also provide new slight for time series mapping of urban at global or regional scale. E.g., nighttime light data has been successfully used to extract the dynamics of urban expansion in China by Liu et al. (2012) and Xiao et al. (2014) separately. Moreover, these national time series of urban data can be integrated into existing or future global LC maps.

Wetlands, as a class differs greatly in the cover type (forest, grassland, shrubland) also deserve more concerns. Instead of mapping wetlands using optical and thermal satellite data, more attentions should focus on the using of radar data, especially in regions with dense vegetation canopy cover. Low values of water in the optical and infrared bands makes it possible to map the extent of open water bodies, but not water underlying vegetation. Since optical and thermal systems are limited by their inability to penetrate vegetation canopy (Townsend 2001; Henderson and Lewis 2008). As a result, wetland areas derived from optical and thermal data are often lower than actual condition (Niu et al., 2012). While radar data is sensitive to the underlying water in vegetation, the backscattered singles increase significantly when the ground floor is covered by water (Kasischke and Bourgeau-Chavez, 1997; Baghdadi et al., 2001; Martinez and Letoan 2007). Encouragingly, ENVISAT ASAR data has been successfully used in land cover mapping at global scale (Defourny et al., 2016).

Until now, NDVI, EVI, and reflectance data are still three main kinds of satellite data for mapping forests at global scale (Arino et al., 2008; Bontemps et al., 2010; Friedl et al., 2010). One meaningful thing is fully discovering phenological information implied in NDVI and EVI, since the phenological features of five classes of forests are quite different. To this end, the best approach is seeking the optical compositions of NDVI or EVI at different seasons or growing periods (DeFries et al., 1995). In other words, now NDVI and EVI have been widely used to study the phenological features of different forest classes (Ahl et al., 2006; Xiao et al., 2006; Yu and Zhuang 2006; Reed et al., 2009), these phenological features should also serve forest mapping in return. Moreover, tree species mapping at local or regional scale using radar data (DeFries et al., 1995; Lee et al., 2005; Hyde et al., 2006; Balzter et al., 2007; Neumann et al., 2010; Laurin et al., 2013) and hyperspectral data (Buddenbaum et al., 2005; Clark et al., 2005; Schull et al., 2011; Dalponte et al., 2013) received wide attentions over the recent years. This also provides a new opportunity for global LC mapping in the future, at least in regions where forest mapping is inaccurate and difficult using NDVI, EVI, and reflectance data, particular in transition region or mixed region of different classes of forests.

4.3. The need for building shareable reference database

Training database, as one of the crucial input data, has directly effect to supervised classification. As global LC is high diverse, a key requirement of training databases is that it should be geographically comprehensive and includes variation within each class of interest (Friedl et al., 2002). However, training samples used for producing current global LC maps are seriously rare and not uniformly distributed over China (Hansen et al., 2000; Friedl et al., 2010; Tateishi et al., 2014). This means that these training databases are not adequate and could not provide well representation of the diverse LC classes in China. This case also well illustrates the low accuracy of these maps over China.

The same validation database is the basis to compare the accuracies of different LC maps. Since the accuracies of current global LC maps provided by data producers were based on different validation database, it is difficult to judge which one better fit the actual case. Besides, validation database with high quality and representation is a foundation of an unbiased estimation. While, just like training databases, validation database used for accuracy assessment of current global LC maps are also rare and non-uniformly distributed, particularly in China.

However, generation of reference database, including training and validation database, at global scale is a huge project fulfilled with huge challenges. Up to now, reference databases were mainly gained by interpreting middle or high resolution images. Even taking full consideration that, as much as possible LC experts of different regions should participate in interpretation, there were still limited experts could participated in this work. E.g., 18 experts participated in collecting validation database for CCI-LC (Defourny et al., 2016), and 27 experts (23 training databases interpreters, and 4 validation database interpreters) participated in collecting samples for FROM-GLC (Gong et al., 2013). Considering the high diversity of LC classes, these limited experts may be familiar with most regions, but not the whole study area. One typical case is that it is difficult to determine the LC class of one sample belong to grass or bogs/meadows using Landsat or high resolution images alone, if we do not have enough understanding of the sampling region. Under such circumstance, wetlands are often under- or un-sampled in some regions. E.g., wetlands in forms of bogs and meadows are widely distributed in Tibetan Plateau; however, even no one sample of wetlands was collected here in previous global LC mapping activities (Friedl et al., 2010).

Given the above, in order to build shareable and standard reference database at global scale, the first way is using crowdsourcing volunteers in an international network. E.g., build an open online platform like or based on GE, so that more and more people whom are interested in LC mapping or data users can freely and easily participate in this work though the online platform. Second, more efforts should be paid on the integrated using of the existing and forthcoming reference database at global and regional scale (Gong et al., 2013; Tateishi et al., 2014). Before the integration of these reference databases, however, it is necessary to make a full assessment for the characteristics of different reference database, as they may not be suitable for the accuracy assessment for all LC maps (Tsendbazar et al., 2015).

5. Conclusions

The release of several new global LC maps in recent years has greatly enriched data users' choice. These global LC maps also show obvious advantages in depicting detailed features of the Earth surface. In this study, aimed at providing guidelines for the using of existing global LC datasets over China, we made a comprehensive assessment for nine commonly used global LC maps, i.e. IGBP DISCover, UMD, GLC 2000, MCD12Q1 2001 and 2010, GLCNMO 2008, CCI-LC 2000 and 2010, and GlobeLand30 2010. We also summarized several far-reaching lessons from previous studies, and hoped that these discussions will benefit global LC mapping in the future.

The results show that, for all LC maps except GlobeLand30 2010, CCI-LC 2010 has the highest overall accuracy (58.65%), and the second is CCI-LC 2000 (67.10%). The overall accuracy of MCD12Q1 2010 and 2001 is 56.04% and 55.88%, respectively. Next coming are GLC 2000 and GLCNMO 2008, which are 50.14% and 48.76%, respectively. The overall accuracy of IGBP DISCover and UMD are

relatively lower, which are 37.44% and 31.86%, respectively. When five classes of forests were aggregated into forests, the overall accuracies of the eight maps increased in a range of 6.60–14.35%. The overall accuracies of CCI-LC 2010 and 2000 reach to 71.98% and 71.87%, respectively; and they are 70.37.69% and 70.23% for MCD12Q1 2010 and 2001, respectively. For GLC 2000, GLCNMO 2008, IGBP DISCover, and UMD, their overall accuracies reach to 59.35%, 58.04%, 44.34%, and 38.46%, respectively. Overall, the recently released higher spatial resolution global LC maps, i.e. 500-m MCD12Q1 2010/2001 and 300-m CCI-LC 2010/2000, show higher accuracy than those 1-km global LC maps, i.e. GLC 2000, IGBP DISCover, and UMD.

In addition, the overall accuracy of GlobeLand30 2010 over China is 82.39%, which is even slightly higher than its global overall accuracy (80.30%). As a result, this data could be served as a baseline of LC map of China at some degree, if the classification scheme adopted in GlobeLand30 could meet the requirement of application. However, if we are interested in LC maps with more detailed classes, such as including the separation of five classes of forests, CCI-LC and MCD12Q1 could better match the demand.

This study has further shown that there are some regions where local accuracies of global LC maps are quite different, particularly in Da Hinggan Ling, Sichuan Basin, Northern Tibetan Plateau, and Southeast Hills of China. In this case, the local accuracies provided in this study will be a valuable judgement basis for data users who are interested in parts of China.

Although these global LC maps provide valuable data sources for many scientific communities, there are further limitations in using them as time series input data, even those maps produced by same institutes, e.g. CC-LC and MCD12Q1. As both of them have failed in revealing the change trend of some key classes in the past decades of China, including urban and built-up, snow and ice, permanent wetlands, and water bodies, while these classes are key indicators to monitor and model global (climate) change. Thus, future maps should further aimed to derive time series data of these key classes, if we hope to use them as input data of time series model.

Acknowledgments

This work was supported by the National Key Basic Research Program on Global Change (Grant No. 2011CB952001) and the National Natural Science Foundation of China (Grant No. 41671344). The authors thank the team members Lingxiao Wang, Wenbo Zhang, Xiaohui Wang, Xiao Chang, Weiding Feng, and Yufang Zhang for collecting the VSUs. They thank Alexis Comber with the University of Leicester for providing suggestions and literature on spatial analysis methods.

References

Ahl, D.E., Gower, S.T., Burrows, S.N., Shabanov, N.V., Myneni, R.B., Knyazikhin, Y., 2006. Monitoring spring canopy phenology of a deciduous broadleaf forest using MODIS. Remote Sens. Environ. 104, 88–95.

An, Y.M., Zhao, W.W., Zhang, Y.H., 2012. Accuracy assessments of the GLOBCOVER dataset using global statistical inventories and FLUXNET site data. Acta Ecologica Sinica 32, 314–320.

Achard, F., Mollicone, D., Stibig, H.J., Aksenov, D., Laestadius, L., Li, Z., Potapov, P., Yaroshenko, A., 2006. Areas of rapid forest cover change in boreal Eurasia. For. Ecol. Manage. 237, 322–334.

Arino, O., Bicheron, P., Achard, F., Latham, F., Witt, R., Weber, J.L., 2008. GLOBCOVER–the most detailed portrait of Earth. Eur. Space Agency Bullet. 136, 25–31.

Atkinson, P.M., Lewis, P., 2000. Geostatistical classification for remote sensing: an introduction. Comput. Geosci. 26, 361–371.

Baghdadi, N., Bernier, M., Gauthier, R., Neeson, I., 2001. Evaluation of C-band SAR data for wetlands mapping. Int. J. Remote Sens. 22, 71–88.

Balzter, H., Rowland, C.S., Saich, P., 2007. Forest canopy height and carbon estimation at Monks Wood National Nature Reserve, UK, using dual-wavelength SAR interferometry. Remote Sens. Environ. 108, 224–239.

Bartalev, S.A., Belward, A.S., Erchov, D.V., Isaev, A.S., 2003. A new SPOT4-Vegetation derived land-cover map of Northern Eurasia. Int. J. Remote Sens. 24, 1977–1982.

Bartholomé, E., Belward, A., 2005. GLC2000: a new approach to global land cover mapping from Earth observation data. Int. J. Remote Sens. 26, 1959–1977.

Bicheron, P., Amberg, V., Bourg, L., Petit, D., Huc, M., Miras, B., Brockmann, C., Hagolle, O., Delwart, S., Ranera, F., Leroy, M., Arino, O., 2011. Geolocation assessment of MERIS GlobCover orthorectified products. IEEE Trans. Geosci. Remote Sens. 49, 2972–2982.

Bicheron, P., Defourny, P., Brockmann, C., Schouten, L., Vancutsem, C., Huc, M., Bontemps, S., Leroy, M., Achard, F., and Herold, M., 2008. Globcover-products description and validation report. European Space Agency.

Bontemps, S., Defourny, P., Bogaert, E. V., Arino, O., Kalogirou, V., Perez, J.R., 2010. GLOBCOVER 2009 Products Description and Validation Report. European Space Agency.

Buddenbaum, H., Schlerf, M., Hill, J., 2005. Classification of coniferous tree species and age classes using hyperspectral data and geostatistical methods. Int. J. Remote Sens. 26, 5453–5465.

Campbell, J., 1981. Spatial correlation effects upon accuracy of supervised classification of land cover. Photogram. Eng. Remote Sens. 47, 355–364.

Chen, J., Chen, J., Liao, A., Cao, X., Chen, L., Chen, X., He, C., Han, G., Peng, S., Lu, M., 2015. Global land cover mapping at 30m resolution: a POK-based operational approach. ISPRS J. Photogram. Remote Sens. 103, 7–27.

Clark, M.L., Aide, T.M., Grau, H.R., Riner, G., 2010. A scalable approach to mapping annual land cover at 250 m using MODIS time series data: a case study in the Dry Chaco ecoregion of South America. Remote Sens. Environ. 114, 2816–2832.

Clark, M.L., Roberts, D.A., Clark, D.B., 2005. Hyperspectral discrimination of tropical rain forest tree species at leaf to crown scales. Remote Sens. Environ. 96, 375–398.

Cleveland, W.S., 1979. Robust locally weighted regression and smoothing scatterplots. J. Am Stat. Assoc. 74, 829–836.

Colditz, R.R., López Saldaña, G., Maeda, P., Espinoza, J.A., Tovar, C.M., Hernández, A. V., Benítez, C.Z., Cruz López, I., Ressl, R., 2012. Generation and analysis of the 2005 land cover map for Mexico using 250m MODIS data. Remote Sens. Environ. 123, 541–552.

Comber, A., Fisher, P., Brunsdon, C., Khmag, A., 2012. Spatial analysis of remote sensing image classification accuracy. Remote Sens. Environ. 127, 237–246.

Congalton, R., Gu, J., Yadav, K., Thenkabail, P., Ozdogan, M., 2014. Global land cover mapping: a review and uncertainty analysis. Rem. Sens. 6, 12070–12093.

Congalton, R.G., 1988. Using spatial autocorrection analysis to explore the errors in map generated from remotely sensed data. Photogram. Eng. Remote Sens. 54. 587-292.

Dalponte, M., Orka, H.O., Gobakken, T., Gianelle, D., Næsset, E., 2013. Tree species classification in boreal forests with hyperspectral data. IEEE Trans. Geosci. Remote Sens. 51, 2632–2645.

Danko, D.M., 1992. The digital chart of the world project. Photogram. Eng. Rem. Sens. 58, 1125–1128.

Defourny, P., Kirches, G., Brockmann, C., Boettcher, M., Peters, M., Bontemps, S., Lamarche, C., Schlerf, M., Santoro. M., 2016. Land Cover CCI: Product User Guide Version 2. Accessed March 5, 2016. <http://maps.elie.ucl.ac.be/CCI/viewer/download/ESACCI-LC-PUG-v2.5.pdf>.

DeFries, R., Hansen, M., Townshend, J., 1995. Global discrimination of land cover types from metrics derived from AVHRR Pathfinder data. Remote Sens. Environ. 54, 209–222.

Foley, J.A., DeFries, R., Asner, G.P., Barford, C., Bonan, G., Carpenter, S.R., Chapin, F.S., Coe, M.T., Daily, G.C., Gibbs, H.K., 2005. Global consequences of land use. Science 309, 570–574.

Foody, G.M., 2002. Status of land cover classification accuracy assessment. Remote Sens. Environ. 80, 185–201.

Foody, G.M., 2005. Local characterization of thematic classification accuracy through spatially constrained confusion matrices. Int. J. Remote Sens. 26, 1217–1228.

Friedl, M.A., Sulla-Menashe, D., Tan, B., Schneider, A., Ramankutty, N., Sibley, A., Huang, X., 2010. MODIS collection 5 global land cover: algorithm refinements and characterization of new datasets. Remote Sens. Environ. 114, 168–182.

Friedl, M.A., McIver, D.K., Hodges, J.C., Zhang, X., Muchoney, D., Strahler, A.H., Woodcock, C.E., Gopal, S., Schneider, A., Cooper, A., 2002. Global land cover mapping from MODIS: algorithms and early results. Remote Sens. Environ. 83, 287–302.

Fritz, S., See, L., 2008. Identifying and quantifying uncertainty and spatial disagreement in the comparison of global land cover for different applications. Glob. Change Biol. 14, 1057–1075.

Fritz, S., See, L., Rembold, F., 2010. Comparison of global and regional land cover maps with statistical information for the agricultural domain in Africa. Int. J. Remote Sens. 31, 2237–2256.

Gao, H., Jia, G.S., 2012. Spatial and quantitative comparison of satellite-derived land cover products over China. Atmos. Ocean. Sci. Lett. 5, 426–434.

Giri, C., Zhu, Z., Reed, B., 2005. A comparative analysis of the Global Land Cover 2000 and MODIS land cover data sets. Remote Sens. Environ. 94, 123–132.

Gong, P., 2009. Assessment of global land cover map accuracies using Fluxnet location data. Prog. Nat. Sci. 19, 754–759 (in Chinese).

Gong, P., Wang, J., Yu, L., Zhao, Y.C., Zhao, Y.Y., Liang, L., Niu, Z.G., Huang, X.M., Fu, H. H., Liu, S., Li, C.C., Li, X.Y., Fu, W., Liu, C., Xu, Y., Wang, X.Y., Cheng, Q., Hu, L.Y., Yao, W.B., Zhang, H., Zhu, P., Zhao, Z.Y., Zhang, H.Y., Zheng, Y.M., Ji, L.Y., Zhang, Y. E., Chen, H., Yan, A., Guo, J.H., Yu, L., Wang, L., Liu, X.J., Shi, T.T., Zhu, M.H., Chen, Y.L., Yang, G.W., Tang, P., Xu, B., Giri, C., Clinton, N., Zhu, Z.L., Chen, J., Chen, J., 2013. Finer resolution observation and monitoring of global land cover: first

mapping results with Landsat TM and ETM+ data. Int. J. Remote Sens. 34, 2607–2654.
Gong, P., Yu, L., Li, C., Wang, J., Liang, L., Li, X., Ji, L., Bai, Y., Cheng, Y., Zhu, Z., 2016. A new research paradigm for global land cover mapping. Ann. GIS 22, 87–102.
Hansen, M.C., Defries, R.S., Townshend, J.R.G., Sohlberg, R., 2000. Global land cover classification at 1 km spatial resolution using a classification tree approach. Int. J. Remote Sens. 21, 1331–1364.
Hansen, M.C., Reed, B., 2000. A comparison of the IGBP DISCover and University of Maryland 1 km global land cover products. Int. J. Remote Sens. 21, 1365–1373.
Henderson, F.M., Lewis, A.J., 2008. Radar detection of wetland ecosystems: a review. Int. J. Remote Sens. 29, 5809–5835.
Herold, M., Mayaux, P., Woodcock, C.E., Baccini, A., Schmullius, C., 2008. Some challenges in global land cover mapping: an assessment of agreement and accuracy in existing 1 km datasets. Remote Sens. Environ. 112, 2538–2556.
Hou, X.Y., 2001. 1:1000000 Vegetation Map of China. Science Press, Beijing.
Hyde, O., Dubayah, R., Walker, W., Blair, J.B., Hofton, M., Hunsaker, C., 2006. Mapping forest structure for wildlife habitat analysis using multi-sensor (LiDAR, SAR/INSAR, ETM+, Quickbird) synergy. Remote Sens. Environ. 102, 63–73.
Jung, M., Henkel, K., Herold, M., Churkina, G., 2006. Exploiting synergies of global land cover products for carbon cycle modeling. Remote Sens. Environ. 101, 534–553.
Kasischke, E.S., Bourgeau-Chavez, L.L., 1997. Monitoring South Florida wetlands using ERS-1 SAR imagery. Photogram. Eng. Rem. Sens. 63, 281–291.
Kuenzer, C., Leinenkugel, P., Vollmuth, M., Dech, S., 2014. Comparing global land-cover products–implications for geoscience applications: an investigation for the trans-boundary Mekong Basin. Int. J. Remote Sens. 35, 2752–2779.
Kyriakidis, P.C., Dungan, J.L., 2001. A geostatistical approach for mapping thematic classification accuracy and evaluating the impact of inaccurate spatial data on ecological model predictions. Environ. Ecol. Stat. 8, 311–330.
Kyriakidis, P.C., Shortridge, A.M., Goodchild, M.F., 1999. Geostatistics for conflation and accuracy assessment of digital elevation models. Int. J. Geograp. Inform. Sci. 13, 677–707.
Latifovic, R., Olthof, I., 2004. Accuracy assessment using sub-pixel fractional error matrices of global land cover products derived from satellite data. Remote Sens. Environ. 90 (2), 153–165.
Laurin, G.V., Liesenberg, V., Chen, Q., Guerriero, L., Del Frate, F., Bartolini, A., Coomes, D., Wilebore, B., Lindsell, J., Valentini, R., 2013. Optical and SAR sensor synergies for forest and land cover mapping in a tropical site in West Africa. Int. J. Appl. Earth Obs. Geoinf. 21, 7–16.
Lee, J., Grunes, M., Ainsworth, T., Hajnsek, I., Mette, T., Papathanassiou, K., 2005. Forest classification based on L-band polarimetric and interferometric SAR data. ESA Special Publ. 586, 1–6.
Li, Y.C., Gong, P., Chen, J., Liu, C.X., He, C.Y., 2005. Landscape pattern and its dynamical change in north China during 1989–1999. J. Soil Water Conserv. 19, 143–146 (in Chinese).
Liu, Z., He, C., Zhang, Q., Huang, Q., Yang, Y., 2012. Extracting the dynamics of urban expansion in China using DMSP-OLS nighttime light data from 1992 to 2008. Landsc. Urban Plan. 106 (1), 62–72.
Liu, J.Y., Zhang, Z.X., Zhuang, D.F., Wang, Y.M., Zhou, W.C., Zhang, S.W., Li, R.D., Jiang, N., Wu, S.X., 2003. A study on the spatial-temporal dynamic changes of land-use and driving forces analyses of China in the 1990s. Geograp. Res. 22, 1–12 (in Chinese).
Liu, J.Y., Kuang, W.H., Zhang, Z.X., Xu, X.L., Qin, Y.W., Ning, J., Zhou, W.C., Zhang, S. W., Li, R.D., Yan, C.Z., Wu, S.X., Shi, X.Z., Jiang, N., Yu, D.S., Pan, X.Z., Chi, W.F., 2014. Spatiaotemporal characteristics, patterns and causes of land-use changes in China since the late 1980s. J. Geog. Sci. 24 (2), 195–210.
Loveland, T.R., Belward, A.S., 1997. The IGBP-DIS global 1 km land cover data set, DISCover: first results. Int. J. Remote Sens. 18, 3289–3295.
Loveland, T.R., Reed, B.C., Brown, J.F., Ohlen, D.O., Zhu, Z., Yang, L., Merchant, J.W., 2000. Development of a global land cover characteristics database and IGBP DISCover from 1 km AVHRR data. Int. J. Remote Sens. 21, 1303–1330.
Martinez, J., Letoan, T., 2007. Mapping of flood dynamics and spatial distribution of vegetation in the Amazon floodplain using multitemporal SAR data. Remote Sens. Environ. 108, 209–223.
Maselli, F., Conese, C., Petkov, L., 1994. Use of probability entropy for the estimation and graphical representation of the accuracy of maximum likelihood classifications. ISPRS J. Photogram. Rem. Sens. 49, 13–20.
Mayaux, P., Eva, H., Gallego, J., Strahler, A.H., Herold, M., Agrawal, S., Naumov, S., De Miranda, E.E., Di Bella, C.M., Ordoyne, C., 2006. Validation of the global land cover 2000 map. IEEE Trans. Geosci. Remote Sens. 44, 1728–1739.
McCallum, I., Obersteiner, M., Nilsson, S., Shvidenko, A., 2006. A spatial comparison of four satellite derived 1km global land cover datasets. Int. J. Appl. Earth Obs. Geoinf. 8, 246–255.
Meer, F.V.D., 1996. Classification of remotely-sensed imagery using an indicator kriging approach: application to the problem of calcite-dolomite mineral mapping. Int. J. Remote Sens. 17, 1233–1249.
Niu, Z.G., Shan, Y.X., Zhang, H.Y., 2012. Accuracy assessment of wetland categories from the GlobCover2009 data over China. Wetland Sci. 10, 389–395 (in Chinese).
Neumann, M., Ferro-Famil, L., Reigber, A., 2010. Estimation of forest structure, ground, and canopy layer characteristics from multibaseline polarimetric interferometric SAR data. IEEE Trans. Geosci. Remote Sens. 48, 1086–1104.
Pérez-Hoyos, A., García-Haro, F.J., San-Miguel-Ayanz, J., 2012a. Conventional and fuzzy comparisons of large scale land cover products: application to CORINE, GLC2000, MODIS and GlobCover in Europe. ISPRS J. Photogram. Rem. Sens. 74, 185–201.
Pérez-Hoyos, A., García-Haro, F.J., San-Miguel-Ayanz, J., 2012b. A methodology to generate a synergetic land-cover map by fusion of different land-cover products. Int. J. Appl. Earth Obs. Geoinf. 19, 72–87.
Ran, Y.H., Li, X., Lu, L., 2010. Evaluation of four remote sensing based land cover products over China. Int. J. Remote Sens. 31, 391–401.
Reed, B.C., Schwartz, M.D., Xiao, X., 2009. Remote sensing phenology: status and the way forward. In: Noormets, A. (Ed.), Phenology of Ecosystem Processes. Springer, New York, pp. 231–246.
Running, S.W., 2008. Ecosystem disturbance, carbon, and climate. Science 321, 652–653.
Scepan, J., Menz, G., Hansen, M.C., 1999. The DISCover validation image interpretation process. Photogram. Eng. Rem. Sens. 65, 1075–1081.
Sedano, F., Gong, P., Ferrao, M., 2005. Land cover assessment with MODIS imagery in southern African Miombo ecosystems. Remote Sens. Environ. 98, 429–441.
Schneider, A., Friedl, M.A., Potere, D., 2009. A new map of global urban extent from MODIS satellite data. Environ. Res. Lett. 4 (4), 2–12.
Schneider, A., Friedl, M.A., Potere, D., 2010. Mapping global urban areas using MODIS 500-m data: new methods and datasets based on 'urban ecoregions'. Remote Sens. Environ. 114 (8), 1733–1746.
Schull, M.A., Knyazikhin, Y., Xu, L., Samanta, A., Carmona, P.L., Lepine, L., Jenkins, J., Ganguly, S., Myneni, R., 2011. Canopy spectral invariants, Part 2: Application to classification of forest types from hyperspectral data. J. Quant. Spectrosc. Radiat. Transfer 112, 736–750.
Steele, B.M., Winne, J.C., Redmond, R.L., 1998. Estimation and mapping of misclassification probabilities for thematic land cover maps. Remote Sens. Environ. 66, 192–202.
Stibig, H.J., Achard, F., Fritz, S., 2004. A new forest cover map of continental Southeast Asia derived from SPOT- VEGETATION satellite imagery. Appl. Veg. Sci. 7 (2), 153–162.
Strahler, A.H., Boschetti, L., Foody, G.M., Friedl, M.A., Hansen, M.C., Herold, M., Mayaux, P., Morisette, J.T., Stehman, S.V., Woodcock, C.E., 2006. Global Land Cover Validation: Recommendations for Evaluation and Accuracy Assessment of Global Land Cover Maps. European Communities, Luxembourg.
Tateishi, R., Hoan, N.T., Kobayashi, T., Alsaaideh, B., Tana, G., Phong, D.X., 2014. Production of global land cover data-GLCNMO2008. J. Geograp. Geol. 6 (3), 99–123.
Tchuenté, A.T.K., Roujean, J.L., De Jong, S.M., 2011. Comparison and relative quality assessment of the GLC2000, GLOBCOVER, MODIS and ECOCLIMAP land cover data sets at the African continental scale. Int. J. Appl. Earth Obs. Geoinf. 13 (2), 207–219.
Townsend, P.A., 2001. Mapping seasonal flooding in forested wetlands using multi-temporal Radarsat SAR. Photogram. Eng. Rem. Sens. 67, 857–864.
Tsendbazar, N.E., Bruin, S., Herold, M., 2015. Assessing global land cover reference datasets for different user communities. ISPRS J. Photogram. Rem. Sens. 10 (3), 93–114.
van Oort, P.A.J., Bregt, A.K., de Bruin, S., de Wit, A.J.W., Stein, A., 2004. Spatial variability in classification accuracy of agricultural crops in the Dutch national land-cover database. Int. J. Geograp. Inform. Sci. 18, 611–626.
Wu, W.B., Shibasaki, R., Yang, P., Ongaro, L., Zhou, Q., Tang, H., 2008. Validation and comparison of 1 km global land cover products in China. Int. J. Remote Sens. 29, 3769–3785.
Xiao, P.F., Wang, X.H., Feng, F.Z., Zhang, X.L., Yang, Y.K., 2014. Detecting China's urban expansion over the past three decades using nighttime light data. IEEE J. Select. Topics Appl. Earth Observ. Rem. Sens. 7 (10), 4095–4105.
Xiao, X., Hagen, S., Zhang, Q., Keller, M., Moore, B., 2006. Detecting leaf phenology of seasonally moist tropical forests in South America with multi-temporal MODIS images. Remote Sens. Environ. 103, 465–473.
Xu, W.T., Wu, B.F., Yan, C.Z., Huang, H.P., 2005. China land cover 2000 using SPOT VGT S10 data. J. Rem. Sens. 9, 204–304 (in Chinese).
Yu, L., Wang, J., Gong, P., 2013. Improving 30 m global land-cover map FROM-GLC with time series MODIS and auxiliary data sets: a segmentation-based approach. Int. J. Remote Sens. 34, 5851–5867.
Yu, X., Zhuang, D., 2006. Monitoring forest phenophases of Northeast China based on MODIS NDVI data. Resour. Sci. 28, 111–117.
Zhang, Z.X., Wang, X., Zhao, X.L., Liu, B., Yi, L., Zuo, L.J., Wen, Q.K., Liu, F., Xu, J.Y., Hu, S.G., 2014. A 2010 update of national land use/cover database of China at 1:100000 scale using medium spatial resolution satellite images. Remote Sens. Environ. 149, 142–154.